

Final Report
NASA Grant NSG-7189

A Comparison of Two Types of Velocity Models for the
Lunar Crust: Smooth, Continuous and Stepwise Layered

Prepared by

Anthony F. Gangi

Department of Geophysics

Texas A&M University

College Station, Texas 77843

(NASA-CR-157830) A COMPARISON OF TWO TYPES
OF VELOCITY MODELS FOR THE LUNAR CRUST:
SMOOTH CONTINUOUS AND STEPWISE LAYERED
Final Report, 1 Feb. 1976 - 15 Mar. 1978
(Texas A&M Univ.) 59 p HC A04/MF A01
for

N79-12987

Unclas
G3/91 37999

National Aeronautics and Space Administration

Lunar Programs Office

NASA Headquarters, Code SM

Washington, D.C. 20546

1 November, 1978

Grant Period: 1 Feb. 1976 to 15 Mar. 1978



Table of Contents

Abstract	i
Introduction —	1
Apollo-14 and -16 ASE Data	5
Results	9
Traveltimes	10
Amplitudes	13
Geophone-Coupling and Shot-Strength Variability	17
Summary	23
Appendix A, Variation in amplitude with distance in a vertically inhomogeneous medium;	27
Appendix B, The relative geophone sensitivities, shot strengths and amplitude variation; least-squares analysis.	31
References	35
Table I. Correspondence of binary data values (B.D.) with Geophone voltage (V). (Geophone 1, Apollo 16)	37
Table II. Shot-to-Geophone Separations	38
Table III. Traveltimes (milliseconds)	39
Table IV. Amplitude Data (arbitrary units)	40
Table V. Data Weights and Separations; Apollo-16 ASE	41
List of Figure Captions	42

Final Report, NASA Grant NSG-7189

Abstract

A Comparison of Two Types of Velocity Models for the
Lunar Crust: Smooth, Continuous and Stepwise Layered

Anthony F. Gangi
Department of Geophysics
Texas A&M University

The data from the Apollo-14 and Apollo-16 Active Seismic Experiments have been reanalyzed and show that a power-law velocity variation with depth, $v(z) \approx 110z^{1/6}$ m/sec ($0 < z < 10$ m), is consistent with both the travel-times and amplitudes of the first arrivals for source-to-geophone separations up to 32m. The data were improved by removing spurious glitches, filtering and stacking. While this improved the signal-to-noise ratios, it was not possible to measure the arrival times or amplitudes of the first arrivals beyond 32m. The data quality precludes a definitive distinction between the power-law velocity variation and the layered-velocity model proposed previously. However, the physical evidence that the shallow lunar regolith is made up of fine particles adds weight to the 1/6-power velocity model because this is the variation predicted theoretically for self-compacting spheres.

The 1/6-power law predicts the traveltime, $t(x)$, varies with separation, x , as $t(x) = t_0(x/x_0)^{5/6}$ and, using a first-order theory, the amplitude,

$A(x)$, varies as $A(x) = A_0(x/x_0)^{(13-m)/12}$, $m > 1$; the layer-velocity model predicts $t(x) = t_0(x/x_0)$ and $A(x) = A_0(x/x_0)^2$, respectively. The measured exponents for the arrival times were between 0.63 and 0.84 while those for the amplitudes were between -1.5 and -2.2. The large variability in the amplitude exponent is due, in part, to the coarseness with which the amplitudes are measured (only five bits are used per amplitude measurement) and the variability in geophone sensitivity and thumper-shot strengths.

A least-squares analysis was devised which uses redundancy in the amplitude data to extract the geophone sensitivities, shot strengths and amplitude exponent. The method was used on the Apollo-16 ASE data and it indicates there may be as much as 30 to 40% variation in geophone sensitivities (due to siting and coupling effects) and 15 to 20% variability in the thumper-shot strengths. However, because of the low signal-to-noise ratios in the data, there is not sufficient accuracy or redundancy in the data to allow high confidence in these results.

Introduction. The first lunar seismograms recorded by the Apollo-11 seismometers (Latham, et al., 1970a,b) surprised many seismologists. Their unusually long durations (see Figure 1) gave rise to numerous theoretical speculations. Proposed mechanisms ranged from secondary-ejecta effects (Latham, et al., 1970a; Chang, et al., 1970; Mukhamedzhanov, 1970) to scattering of the waves by shallow internal fractures and inhomogeneities (Latham, et al., 1970a,b) or by topographic irregularities (Gold and Soter, 1970). It soon became clear that the secondary-ejecta mechanisms were not viable ones because the same long duration occurred for seismograms from moonquakes with foci in the lunar interior.

Early data indicated that the compressional-wave velocity was very low near the lunar surface (~ 0.1 km/sec; Latham, et al., 1970c, Sutton and Duennebier, 1970) and increased to approximately 6 km/sec at a depth of 20 kilometers (Latham, et al., 1970d). Latham, et al. (1970a,b) showed that the variation of the amplitude envelope with time and distance was consistent with a diffusive-scattering mechanism provided the Q of the medium was greater than 3000.

Gold and Soter (1970) interpreted the Apollo-12 data to imply that the shallow lunar crust consisted of a deep layer of powder. They assumed a linear velocity variation with depth and, through computer simulation using ray acoustics, they were able to approximate the actual signal very well. They showed that the long duration could be explained by scattering of the nearly vertically-incident waves by topographic irregularities (Figure 2). They also showed that the seismic amplitudes are greatly enhanced in such a medium, so that it required less power to transmit seismic waves than previously believed.

Kovach, et al. (1971) proposed a layered model with a stepwise increasing velocity variation based on the data of the Active Seismic Experiment (ASE) at the Apollo-14 landing site. They obtained a p-wave velocity (V_p) of 104 m/sec for a top layer of 8.5 meters thickness and a $V_p = 229$ m/sec for an underlying layer (the Fra Mauro formation) of 38 to 76 meters thickness. A similar model was used to interpret the Apollo-16 ASE data and gave a $V_p = 114$ m/sec for a 12.2-meter-thick top layer and a $V_p = 250$ m/sec for an underlying layer 70-meters thick (Kovach, et al., 1972).

Gangi (1972) proposed a self-compacting-powder model which gives a velocity varying as the sixth root of the depth; in this model the velocity at the lunar surface goes to zero. This, in turn, gives a long duration to the signal by scattering from topographic irregularities, very low correlation between horizontal and vertical displacements, a changing signal envelope that varies with source-to-receiver separation and a varying spectrum over the signal duration. These effects have been noted by Latham et al. (1970c, 1970d) and they also are explained by the diffusive scattering model (Latham, et al., 1970c) and the surface-irregularity scattering model (Gold and Soter, 1970).

Kovach and Watkins (1973) extended and refined the layered model by incorporating the traveltime of the Apollo-14 Lunar-Module ascent. However, they pointed out that: "the exact details of the velocity variation in the upper 5-10 km of the Moon cannot yet be resolved (i.e., whether it is smooth as depicted or a stepwise increase) but one simple observation can be made. Self-compression of any rock powder such as the Apollo 11 or 12 soils or terrestrial sands cannot duplicate

the observed magnitude of the lunar velocity change and the steep velocity-depth gradient ($\sim 2 \text{ km s}^{-1} \text{ km}^{-1}$). However, it is not expected that a self-compacting-powder layer of 5 km thick would exist on the Moon; if such a layer exists, it would be, most likely, thinner than 1 km and probably thinner than 100 m.

Dainty, et al. (1974) performed a detailed analysis of the diffusive-scattering mechanism and compared their theoretical results both with lunar data and seismic-modelling data. They showed they could match the envelopes of the lunar seismograms using this theory if, for a frequency of 0.45 Hz, the apparent thickness of the scattering layer is 25 km, the mean distance between scatterers at the base of the layer is ~ 5 km and the Q of the medium is 5000. The corresponding values for a frequency of 1.0 Hz are: 14-km scattering-layer thickness, ~ 2 km between scatterers and a Q of 5000. The thicknesses of the scattering layer (and its variability with frequency) seem to be inordinately large and may indicate that the model used is not appropriate for the lunar crust. A similar analysis should hold for body-wave scattering by topographic irregularities; in this case, the scattering-layer thickness would correspond to the surface area over which the nearly vertically-incident waves are efficiently scattered and the spacing between scatterers in the layer would correspond to the spacing between surface scatterers (of wave-length size).

Cooper, et al. (1974) used the data of the Active Seismic Experiments of Apollo 14 and 16 along with the Lunar Seismic Profiling Experiment (LSPE) data of Apollo 17 and other man-made impacts to obtain a model of the velocity structure of the shallow lunar crust.

They assumed a layered model and assumed that the first arrivals (beyond about 10 m) were seismic refractions. They found their travel-time data were consistent with a five-layer model in which the velocity is: 1) 100 m/sec in the top layer of 4-m thickness, 2) 327 m/sec in the next layer to a depth of 32 m (thickness of 28 m), 3) 495 m/sec to a depth of 390 m, 4) 960 m/sec to a depth of 1385 m and 5) 4700 m/sec for a depth down to at least 1800 m. However, this last velocity is determined from a single source (the LM impact) at distances of the order of 8.7 km from the geophone array (four geophones). The shallower structure is obtained from the traveltime data resulting from the eight explosive-package detonations and the LM ascent; all these sources are within 3 km of the geophone array. Cooper, et al. (1974) show these data can be fitted well with a continuous, linearly-increasing velocity with depth, z ; namely, $V \approx 395 + 778 z$ (m/sec) for z in meters. They also state that "Various power law velocity models can be made to fit the observed data ..." when only the explosive-package and LM-ascent data are used.

It is clear there is still some question regarding the velocity variation with depth in the shallow lunar crust ($z < 1$ km). Since the shallow lunar crust severely modifies the received signals, even those from large distances, it is important to know this shallow velocity variation well. Therefore, it is worthwhile to reanalyze the data to determine which velocity variation with depth is the most probable. The data from the Apollo-14 and Apollo-16 ASE's have been reanalyzed the the results are given below.

Apollo-14 and -16 ASE Data. The data used in this analysis are from the astronaut-activated thumper device of the Apollo-14 and Apollo-16 ASE's. In both experiments, three geophones were sited on the surface in a linear array with 45.72 m (150 ft) spacing between geophones (Lauderdale and Eichelman, 1974). The thumper device was fired at 4.57 m (15 ft) intervals between the ends of the arrays (see Figure 3). Firings (shots) 5, 6, 8, 9, 10, 14, 15 and 16 of the Apollo-14 ASE misfired and no data are available for them. For the Apollo-16 ASE, two shots were omitted between geophones 1 and 2; namely, those at the 4.57 m spacing from the two geophones.

The signals from the geophones are sampled every 1.887 msecs, corresponding to a Nyquist frequency of about 265 Hz. Because of data transmission limitations, a trade-off between sampling rate and the number of bits per sample had to be made. The result was that only five bits were available for each sample. In order to cover the maximum possible dynamic range with only 32 possible binary numbers, the seismic signals were log compressed for large signal levels. The correspondence of the binary-data values (0-31) and the voltage from geophone 1, Apollo 16 is shown in Table I. The other geophone voltages have similar correspondences with the binary data. With only 32 levels possible for the geophone output voltage, the resulting traces will have a coarse character. This makes it difficult to obtain accurate amplitude information if no processing or filtering is performed on the data. Fortunately, it is possible to process the data to obtain reasonably accurate amplitude values.

In order to achieve meaningful results from the analysis, it was necessary to improve the original ASE data. Figure 4 shows three representative traces of the raw data from the Apollo-16 ASE. These data are from the tenth thumper shot and the source-to-receiver separations are 50.29 m (165 ft), 4.57 m (15 ft) and 41.14 m (135 ft) for geophones 1, 2 and 3 respectively. The thumper-firing time is 1.2 seconds after the beginning of the traces. While a high signal-to-noise ratio (S/N) exists for the shortest separation, the S/N for the other two traces is so low that it is difficult, if not impossible, to pick the first arrivals or to measure their amplitudes. In addition, geophone 1 shows severe "glitches", most of which are almost uniformly spaced in time and of uniform amplitude but there are others of varying amplitude and times of occurrence. Similar large glitches are seen on the other two traces. A close look at the data showed that there are smaller glitches throughout the records; these are recognized by the fact that they are of short duration -- generally, only one or two samples -- and had values which were inconsistent with preceding and following sample values.

The first data-improving operation performed was to go through the data by hand and remove the extraneous values and replace them by values interpolated from neighboring values. A computer program was not used in this process because: 1) there are relatively few glitches (excluding the regular, periodic ones in geophone 1, there are fewer than 1%), 2) the coarseness of the amplitude values precludes automatic, computer interpolation and 3) a number of different criteria were used simultaneously to identify and correct the bad sample values.

The result of the "deglitching" process is shown in Figure 5 for the same traces shown in Figure 4. While this improved the records considerably, it is clear the S/N ratios for the geophone-1 and -3 traces are still too low to allow positive identification of the first arrivals.

To improve the S/N and smooth out the traces, the data were bandpass filtered with a four-pole, anti-aliased, Butterworth filter (~12 db/octave slopes at both low and high frequencies) which had 3-db frequencies at 10.5 Hz and 66.25 Hz. The result, for the same three traces, are shown in Figure 6. While this improved the S/N significantly and improved the character of the traces (compare Figures 5 and 6), the S/N for separations larger than 9.14 m (30 ft) was still low because of the decrease in the direct arrival's amplitude.

Spectral analyses of the seismic traces were made to determine the frequency band of the seismic energy and to see if there was significant aliasing of the data. The amplitude spectrum (for geophone 2, shot 10, Apollo-16 ASE) of the first two seconds (1024 samples) is shown in Figure 7. While only half of the full amplitude spectrum (0 to 265 Hz) is shown there, it is clear that there is little, if any, aliasing because most of the signal energy is contained between 10 and 90 Hz with the major part between 10 and 40 Hz. This is the spectrum of the middle trace shown in Figures 4, 5 and 6.

To further improve the data, the traces with the same source-to-receiver separation for both ASE's were summed (or "stacked") together. The implicit assumptions being made here are: (1) the velocity variation with depth is the same at both the Apollo-14 and -16 sites and (2) there is lateral homogeneity for the direct waves at both

sites. The first assumption is reasonably consistent with the results found by Kovach, et al. (1971) for the two sites; the second assumption is consistent with the equivalent assumption made by Kovach, et al. (1971) in their interpretation of the data at each site.

The traces that had the same source-to-receiver separation are listed in Table II for both the Apollo-14 and -16 ASE's. The thumper-shot numbers, corresponding to the given shot-to-geophone separations, are listed in the right half of the table. Among the two experiments, there were between 4 and 7 traces with the same separation. If the background noise is random and the assumptions cited hold, the stacking should give improvements in S/N between 2 and $\sqrt{7}$. The resulting sum signals were amplified so that the peak excursions would be plotted almost full scale for each trace. A representative result is shown in Figure 8. The second trace in Figure 8 is at the same separation as the middle traces in Figures 4, 5 and 6 (i.e., the geophone-2 trace for the 10th thumper shot of the Apollo-16 ASE). For this trace, the S/N improvement should be better than a factor of 2; however, this degree of improvement was not achieved. Nevertheless, improvements in S/N were achieved for this trace, and for the other traces at larger separations, by the stacking technique.

The result of summing the deglitched traces is shown in Figure 9. These signals were filtered, before summing, with a 4-pole, anti-aliased, bandpass, Butterworth filter with 3-db frequencies at 20 and 50 Hz. Arrival times can be determined with some certainty for separations up to 32.00 m (105 ft); it is difficult, if not impossible, to pick arrivals beyond that distance.

One of the single-geophone profiles (geophone 1, Apollo 16) is shown in Figure 10. Arrival times can be easily picked for separations up to 18.29 m (60 ft) and, with difficulty, for 22.86 m (75 ft) and 27.43 m (90 ft). At 32.00 m separation (105 ft), the first arrival is buried in the noise. We were not able to determine a first arrival with any degree of certainty for separations greater than 32.00 m (105 ft). This is consistent with the finding of Kovach and Watkins (1973) for the thumper shots.

Results. The traveltimes and amplitudes of the direct (first arriving) seismic signals of the Apollo-14 and -16 ASE's were analyzed. The traveltimes and amplitudes for separations up to 32.00 m (105 ft) were obtained both from the summed (stacked) traces and from individual traces. In one case, all the "noise-free" traces from both ASE's were stacked in an attempt to improve the S/N ratio. In two other cases, only the "noise-free" traces from each ASE were stacked to give Apollo-14-only and Apollo-16-only stacked profiles. If there are significant differences in the velocity structure at the two sites, these individual-site stacks would show the difference. Little difference was found, over the 32 m, in the traveltimes for these two stacks. The traveltimes for individual geophone profiles were also measured to test the assumption of lateral homogeneity at each site. The quality of the data precluded any positive conclusion regarding this assumption; however, the improvement in S/N ratio achieved by the various stacking indicate this is a reasonable assumption.

Traveltimes. The traveltimes for five of the cases investigated are listed in Table III. In those cases where the S/N ratio was high (up to and including 18.29 m separation, the traveltimes could be determined to within 1/2 sample time (± 1 msec). However, systematic errors — such as those due to variations in the separations, elevation differences, shot-times, etc. — could be as high as one or two sample times.

Log/log plots of traveltime versus separation were used to test the hypothesis of a power-law velocity variation. It can be shown, using Kaufman's (1953) work, that a velocity variation with depth, z , given by

$$v(z) = v_0 (z/z_0)^n \quad (1)$$

results in a direct-wave traveltime, $t(x)$, with separation, x , given by (see also, Gangi, 1972)

$$t(x) = t_0 (x/x_0)^{1-n} \quad (2)$$

where t_0 is the traveltime corresponding to the separation x_0 and v_0 is the velocity at depth z_0 . This incorporates both the traveltime/separation relationships for a constant-velocity medium ($n=0$) and that for a self-compacting-powder medium ($n=1/6$). Therefore, for the two power-law velocity models ($n=0$ and $n=1/6$), the traveltime curve in a log/log plot would be a straight line whose slope, m , would be determined by the power-law exponent ($m=1-n$).

The slopes of least-squares-fitted straight lines are given in Table III along with the velocity v_0 which corresponds to the velocity extrapolated to $z_0=1$ km. As indicated earlier, it is not expected that

the powdered layer would extend to 1 km; therefore, v_0 is not an estimate of the velocity at that depth but is merely a constant used to characterize the velocity. The depth $z_0=1$ km is chosen only for convenience; the reference depth could have been chosen to be 1 m, in which case, the v_0 's in Table III would be multiplied by $(.001)^{1/6} = 0.3162$. While the measured slopes are variable, they are all consistently lower than $m=1-n=1$, the value that would be obtained for the constant velocity model. The measured values tend to cluster near the value predicted by the self-compacting-powder model; namely, $m=1-1/6=.833$.

The variation in the reference velocity, v_0 , is much greater than that of the slopes; its values vary between 340 and 630 m/sec. The slope of 0.63 and reference velocity of 1200 m/sec for the Apollo-16, geophone-1 profile (column 5, Table III) are not very accurate because there are only three good data points (the traveltimes at 9.14, 13.71 and 18.29 m) for determining these values. It gave the least consistent values for n and v_0 . In computing the least-squares lines, the questionable data were given a weight equal to one-quarter that of the high-S/N data.

Traveltimes were calculated from the Apollo-14 and Apollo-16 velocity models given by Kovach and Watkins (1973). These are shown in columns B and C of Table III. In column A, the traveltimes for a powder-layer model with $v_0=350$ m/sec and $n=1/6$ are tabulated. This latter model was an average model found from all the cases treated when the velocity exponent, n , was constrained to be $1/6$. Overall, there are not large differences between the measured traveltimes and the calculated travel-

times using any of the models. However, the biggest differences between the Kovach and Watkins models and the measured values occur at the small separations, precisely where the S/N ratios are highest and where the traveltimes can be picked with the greatest certainty. Their models can be made to fit the close-in data simply by introducing a thin, lower velocity layer at the surface. But it should be recalled that they already have low velocities for the top layers (104 and 114 m/sec for Apollo-14 and -16, respectively) which are relatively thin (8.5 and 12.2 m, respectively).

The traveltime data for the combined Apollo-14 and -16 stacked traces (column 1, Table III) are shown in Figure 11 along with the least-squares-fitted line. These data are from the deglitched traces which have been bandpass filtered with a fourth-order, Butterworth filter having 3-db points at 3 and 66 Hz. It can be seen from Figure 11 that the straight line is an excellent fit to the data and that it would be difficult to change the slope from its given value (0.76) to 1.0, the latter value corresponding to the constant-velocity model. Equally good fits of data points to straight lines were found for the Apollo-14-only and Apollo-16-only stacked data.

Amplitudes. The traveltimes of the first arrivals over the 0-32 m range do not demonstrate a clear distinction between the powered-layer and the layered-velocity models. The data accuracy is such that either model can be accepted. To try to distinguish between the two models, the amplitudes of the first arrivals were measured and compared with the expected distance variation predicted by the two models.

Since the thumper shots give primarily vertical forces and the geophones are vertically oriented, the amplitude of the direct p-wave arrival in the layered model should vary as the inverse square of the separation,

$$A(x) = A_0(x/x_0)^{-2}, \quad (3)$$

for small separations (see, for example, White, 1965, p. 215). On the other hand, for a power-law velocity model, the amplitude variation with separation is given by (see Appendix A)

$$A(x) = \left[-\frac{S(p)}{2\pi x} \frac{d^2 t}{dx^2} \right]^{1/2}, \quad (4)$$

where $S(p)dp$ is the energy radiated in a bundle of rays having ray parameters lying between $p-dp/2$ and $p+dp/2$, the ray parameter is given by $p = \sin\theta(z)/v(z)$, $\theta(z)$ is the angle between the ray and the vertical (z) direction, $v(z)$ is the velocity variation with depth and t is the traveltime for the ray (with ray parameter, p) which returns to the surface at separation x . For the self-compacting-powder model, the amplitude variation is estimated to be (see Appendix A)

$$A(x) = A_0(x/x_0)^{-(13-m)/12}, \quad m > 1, \quad (5)$$

where m is a measure of the source radiation pattern in the power-law-velocity medium. To insure integrability of

$$E = \int_0^{\infty} S(p) dp,$$

where E is the energy radiated by the thumper source, we find $m > 1$. (see Appendix A). This indicates the amplitude decrease of the direct wave with separation is less in the powder-layer model than that in the constant-velocity model. This is consistent with the conclusion of Gold and Soter (1970) based on their analysis for a linearly increasing velocity with depth.

The determination of the amplitude variation with separation for the Apollo-14 and -16 ASE data is more difficult than determining the traveltime data because of: 1) the coarseness of the amplitude sampling, 2) the variability of the thumper-shot strengths, 3) the variability of the geophone sensitivities (primarily due to siting and coupling of the geophones) and 4) the low S/N ratio for the larger separations. The coarseness of the amplitude data is significantly reduced by the interpolating effect of bandpass filtering. The variability due to the shot strengths, the geophone sensitivities and the low S/N ratio are reduced by the averaging inherent in stacking or summing traces (provided the signals are sufficiently coherent for a given source/receiver separation).

On the basis of the measured arrival times (at least for separations less than 22.86 m -- see Table III), sufficient coherency of the signals exists so that averaging of the amplitudes should be possible by summing of traces. The measured amplitudes are given in Table IV. Both the amplitudes for individual traces and for stacked traces are given. Measurements were made

on data that had been bandpass filtered by anti-aliased, fourth-order Butterworth filters with 3 db frequencies of 3 to 66 Hz and 20 to 40 Hz. It can be seen that there is a great deal of scatter in the data. Some of this is due to the thumper-shot variability and some due to geophone siting, but the major part is due to low S/N ratio and the coarseness of the amplitude data. Straight lines were fitted, by least squares, through the data points (on a log-log graph) and the slopes of these lines are included in Table IV. A representative plot of the amplitude data along with its least-squares-fitted line is shown in Figure 12. This represents one of the most complete sets of amplitude data available for a single geophone; namely, geophone 3 for the Apollo-16 ASE. The original traces were bandpass filtered (3 db frequencies at 3 and 66 Hz) prior to measuring the amplitudes.

Because of the low S/N ratio at the larger separations, it is not certain that a straight line (on a log-log plot) is the appropriate fitting function. While all the data are fairly well fitted by the line in Figure 12 (with a slope equal to -2.01), it is clear that the two largest amplitude values (at 4.57 and 9.14 m), which have the best S/N ratios, suggest a lower slope.

The slopes found for all the cases with fairly good data lie between -1.5 and -2.1. However, the possible errors on these slopes are of the order of ± 0.5 . The fact that the slopes are more negative than -1 and close to -2, the slope predicted by a simple flat-layer model, does not mean the amplitude data verifies that model. From equation (5), the slope predicted ^{by} the powder-layer model would be more positive than -1. However, this equation and the theory used to predict a slope of -2 for the flat-layer model are based on

simplifying assumptions; namely, that all the sources are of equal strength, the geophones are equally coupled to the regolith, there is no attenuation by absorption in either model, there is no energy loss by conversion of p-wave energy into s-wave energy (for the powder-layer model) and there are no scatterers in the lunar regolith. The latter three effects would increase the amplitude loss with distance so that the predicted slopes (-2 for the flat layer and $-(13\text{-m})/12$ for the powder layer) should be considered upper bounds on the measured ones. The variability of the thumper-shot strengths and of the geophones would increase the scatter in the data.

While the amplitude data do not preclude either model conclusively (as they would have if the measured amplitudes decreased more slowly than inversely with separation), they do favor the powder-layer model. All the loss mechanisms lead to a greater decrease in amplitude than predicted by the simple analyses of the two models. However, the amplitude data do not show a more rapid decrease than that predicted for the homogeneous-layer models proposed by Kovach and Watkins (1973) while the data clearly do show a more rapid decrease with separation than that predicted by the simple (first-order) theory for the powder-layer model. This discrepancy in the amplitude variation with distance can not be explained by interference of other waves with the direct wave. For the short separations where amplitude data is available (generally less than 27.43 m), interference from reflected or refracted waves would not affect the amplitudes by interference for the flat-layer models; nor would a velocity discontinuity at a depth greater than about 10 m effect the amplitude results (by the same types of interference) in the powder-layer model.

Geophone-Coupling and Shot-Strength Variability. To eliminate the effects of variability in the geophone coupling and the Thumper-shot strengths, an analysis of the amplitude data was made which determines both the geophone sensitivity (in-place) and the shot strengths as well as the exponent of the amplitude variation when there is sufficient redundancy in the data.

If it is assumed that either the flat-layer model or the powder-layer model is valid, the measured amplitude at a particular geophone due to a particular source will be given by

$$A_{ij} = G_i S_j |x_i - x_j|^m \quad (6)$$

where G_i is the sensitivity of the i -th geophone (including coupling and siting effects) located at x_i , S_j is the strength of the j -th shot located at x_j and m is the exponent of the amplitude variation.

Equation (6) can be normalized to the sensitivity of a particular geophone, say G_1 ($i=1,2$ or 3), and to the strength of a particular shot, say S_j . This normalization is necessary because, quite clearly, each geophone sensitivity can be multiplied by some constant factor and each shot strength divided by the same factor without changing the resulting amplitude.

Letting $G_1 S_j = A_0$, equation (6) becomes

$$A_{ij} = A_0 (G_i/G_1) (S_j/S_j) |x_i - x_j|^m. \quad (7)$$

Equation (7) can be linearized in terms of the relative geophone sensitivities, the relative shot strengths, the exponent m and the arbitrary constant A_0 by taking its logarithm:

$$\log A_{ij} = \log A_0 + \log(G_i/G_1) + \log(S_j/S_j) + m \log|x_i - x_j|$$

or, for convenience in writing,

$$a_{ij} = a_0 + g_i + s_j + mX_{ij} \quad (8)$$

where $a_{ij} = \log A_{ij}$, $X_{ij} = \log|x_i - x_j|$, $g_i = \log(G_i/G_1)$ and $s_j = \log(S_j/S_j)$.

The optimum values, in a least-squares sense, of a_0 , g_i , s_j and m can be determined by minimizing the summed, weighted and squared error

$$E^2(a_0, m, \bar{g}, \bar{s}) = \sum_{i=1}^I \sum_{j=1}^J w_{ij} (a_0 + mX_{ij} + g_i + s_j - a_{ij})^2, \quad (9)$$

as a function of these parameters. The result (see Appendix B) is the matrix equation

$$\bar{a} = \bar{A} \cdot \bar{p} \quad (10)$$

where \bar{a} is a vector whose components depend only upon the measured amplitudes (a_{ij}), the weights (w_{ij}) and the measured separations (X_{ij}); \bar{A} is a square matrix whose components depend only upon the weights and the measured separations while \bar{p} is a vector whose components are the unknown parameters: $g_1, \dots, s_1, \dots, a_0$ and m . (The detailed form of this equation is given in Appendix B). The solution to this matrix equation is

$$\bar{p} = \bar{A}^{-1} \cdot \bar{a}. \quad (11)$$

If there is sufficient redundancy in the data, the matrix will be well conditioned and non-singular and will have a stable inverse.

The weights are established from the quality of the data. The weights

for the Apollo-16 data are shown in Table V. From the table it is seen that only 14 of the 19 thumper shots gave useful amplitude data (shots 1, 11, 13, 14 and 19 were not useable) and, of these 14, only three (shots 6, 7 and 17) give measurable first-arrival amplitudes on more than one geophone. (Shots 12 and 17 gave amplitudes of .89 and .06?, respectively, for the 3-66 Hz bandpassed traces on geophone 2; all other amplitudes are given in Table IV). Therefore, only six amplitude measurements (two for each shot) are available to determine the six parameters a_0 , m , g_1 , g_3 , s_6 , s_{17} (when geophone 2 and shot 7 are used as the reference geophone and shot, respectively). With the relative geophone sensitivities, the constant a_0 and the exponent m set by these data, the remaining relative shot strengths will be determined by the assumed amplitude variation (equation 6 or 7) and the measured amplitude.

Having only six correlative amplitude measurements to determine six unknowns (by means of the linear equations 8 or 10) means there is little redundancy in the amplitude data. Nevertheless, the solution of these six equations in the six unknowns do constitute a least-squares solution. This is because weighting factors are used in the equations; the weights can be interpreted to mean that more than six measurements of equal weight were made, some of which were identical measurements (i.e., same shot location), and the results combined together to give a single result of greater weight.

Using the six available correlative amplitude values, the matrix equation becomes:

$$\begin{bmatrix} \langle w_{ij} \bar{a}_{ij} \rangle \\ \langle w_{ij} \bar{a}_{ij} X_{ij} \rangle \\ \langle w_{1j} \bar{a}_{1j} \rangle \\ \langle w_{3j} \bar{a}_{3j} \rangle \\ \langle w_{i6} \bar{a}_{i6} \rangle \\ \langle w_{i17} \bar{a}_{i17} \rangle \end{bmatrix} = \begin{bmatrix} \langle w_{ij} \rangle & \langle w_{ij} X_{ij} \rangle & \langle w_{1j} \rangle & \langle w_{3j} \rangle & \langle w_{i6} \rangle & \langle w_{i,17} \rangle \\ - & \langle w_{ij} X_{ij}^2 \rangle & \langle w_{ij} X_{ij} \rangle & \langle w_{3j} X_{3j} \rangle & \langle w_{i6} X_{i6} \rangle & \langle w_{i17} X_{i17} \rangle \\ - & - & \langle w_{ij} \rangle & 0 & \langle w_{i6} \rangle & \langle w_{i,17} \rangle \\ - & - & - & \langle w_{3j} \rangle & \langle w_{i6} \rangle & \langle w_{i,17} \rangle \\ - & - & - & - & \langle w_{i6} \rangle & 0 \\ - & - & - & - & - & \langle w_{i,17} \rangle \end{bmatrix} \begin{bmatrix} a_0 \\ m \\ g_1 \\ g_3 \\ s_6 \\ s_{17} \end{bmatrix}$$

where $i = 1, 2$ and 3 and $j = 6, 7, 17$. In terms of assumed values of w_{ij} and the measured values of X_{ij} and a_{ij} , this equation becomes

$$\begin{bmatrix} -3.734 \\ -11.710 \\ -0.211 \\ -1.164 \\ -1.592 \\ -0.914 \end{bmatrix} = \begin{bmatrix} 3.50 & 10.35 & 1.00 & .75 & 1.00 & 1.25 \\ - & 30.84 & 2.62 & 2.39 & 3.13 & 3.48 \\ - & - & 1.00 & 0 & 0 & 1.00 \\ - & - & - & 0.75 & 0.50 & 0 \\ - & - & - & - & 1.00 & 0 \\ - & - & - & - & - & 1.25 \end{bmatrix} \begin{bmatrix} a_0 \\ m \\ g_1 \\ g_3 \\ s_6 \\ s_{17} \end{bmatrix}$$

Solving this matrix equation, the relative geophone sensitivities and relative shot strengths are found to be:

$$G_1/G_2 = .724; \quad G_3/G_2 = 1.40$$

$$S_6/S_7 = .803; \quad S_{17}/S_7 = .848$$

and the exponent is

$$m = -3.57. \quad \text{---}$$

Unfortunately, these values appear to be unreasonable; this is not surprising considering the lack of redundancy and quality in the amplitude data. The 30 to 40% differences in the relative geophone sensitivities are not too unreasonable, but are higher than expected. Also, the 15 to 20% variations in the shot strengths are possible, but again seem large. The value of the exponent ($m = -3.57$) is different by almost a factor of two compared to the values obtained using single-geophone profiles and stacked profiles (compare Table IV). The 30 to 40% differences in geophone sensitivity have no effect on the amplitude variation with distance as determined by a single-geophone profile. The 20% differences in shot strengths (of shots 6 and 17 relative to shot 7) would not cause appreciable differences in the slopes (or exponents) obtained from single-geophone profiles (provided, of course, that these differences are representative of the differences in the other shots). It is concluded that the least-squares analysis given above does not give reliable values for the parameters (m , G_1/G_2 , G_3/G_2 , S_6/S_7 , S_{17}/S_7). However, the method is a valid one and the reason for the unreliability in the parameter values is the lack of redundancy and quality in the data.

While the method is not useful for this data set, it is presented in detail because there may be other instances where it would give valid results. It provides a rationale for the design of seismic experiments which test amplitude variation with separation when variability in source strengths and geophone sensitivities is anticipated (as is generally the case).

The same amplitude analysis could not be performed on the Apollo-14 ASE data because there were no correlative amplitude values for geophones 2 and 3 (due to misfires and poor signal-to-noise ratios).

Summary

The data from the thumper shots of the Apollo-14 and Apollo-16 ASE's have been reanalyzed to test whether the velocity variation in the shallow lunar crust (depths ≤ 10 meters) can be represented by a self-compacting powder layer as proposed by Gold and Soter (1972) and Gangi (1972) or by constant velocity layers as proposed by Kovach et.al. (1971, 1972, 1973).

Both the traveltimes and the amplitudes for the first arrivals were remeasured and compared with the values predicted by the self-compacting-powder-layer model proposed by Gangi ($v(z)=v_0(z/z_0)^{1/6}$) and the layered-velocity model proposed by Kovach, et.al. To improve the quality of the data, they were "deglitched" to remove spurious values and bandpass filtered. Four-pole, anti-aliased Butterworth filters with bandpasses between 3 and 66Hz and 20 and 50Hz (3 db frequencies) were used to improve the signal-to-noise ratio (S/N). In addition, traces from different thumper shots and with the same source-to-geophone spacing were summed together to improve the S/N. While these techniques improved the S/N, it still was not possible to measure traveltimes or amplitudes of the first arrivals for separations greater than 32m.

While there is variability in the results obtained (see Table III), the traveltimes for the direct arrival over a separation of 32m can be fit by the 1/6-power velocity model. The measured values of the exponent for an assumed power-law velocity varied between approximately 1/3 to 1/7; that is, $.67 < 1-n < .86$ (see Table III) where n is the exponent for the depth variation of the velocity. The best (or average) model for both the Apollo-14 and Apollo-16 sites is $v(z) \approx 350(z/z_0)^{1/6}$ m/sec for $z_0 = 1$ km or $v(z) \approx 110z^{1/6}$, $0 \leq z \leq 10$ m. This is

fairly close to the velocity variation, $v(z) \approx 190z^{1/6}$, predicted by Gangi (1972) on the basis of Gassmann's analysis (1953) and the measured mechanical properties of the lunar soil. -

The measured traveltimes of the first arrivals over the 32m separation are in reasonable agreement with the values predicted by the layered model (see Table III). However, the biggest percentage deviations occur at the two shortest distances (4.57 and 9.14m) where the S/N is high and the traveltimes can be measured most accurately. At these separations, the measured arrival times, which are accurate within at least one sample interval (or 1.89 msec), differs from those predicted by the layered model by 10 to 15 msec. The corresponding differences for the power-law model is generally less than 2 msec. While this indicates that the self-compacting-powder-layer model is probably the correct one, the quality of the data precludes a definitive distinction between the two models.

No comparison was made of the measured traveltimes with those predicted by the linear velocity variation used by Gold and Soter (1970), namely, $v(z) = v_0 + az$, because it was an assumed velocity variation which is not based on any physical mechanism. The traveltime relationship for this velocity variation, $t = (2/a) \sinh^{-1}(ax/2v_0)$, should also fit the data to the same accuracy as that of the layered-velocity model. It, too, would have the largest percentage deviations at the shortest distances.

An analysis of the amplitudes of the first arrivals was performed to test the models. The predicted amplitude variation with separation, x - assuming no amplitude loss due to attenuation, scattering or conversion of p-wave energy into s-wave energy - for the layer model is x^{-2} while that for the 1/6-power velocity model is $x^{(13-m)/12}$, $m > 1$. The measured exponent varied

from -1.55 to -2.34 (see Table IV) with the average value near -2.0. While this result, at first glance, seems to favor the constant velocity model, the fact that there will be amplitude loss due to scattering, attenuation and wave-type conversion makes this result more consistent with the power-law model. However, the large errors in the amplitude data — which are more severe than the errors in the arrival times — preclude a definitive conclusion regarding which is the appropriate velocity *model*.

An attempt was made to eliminate the errors in amplitude, due to variations in the geophone sensitivities and shot strengths, by using a least-squares method. The method requires that the signals, from individual shots, be detected on two or more geophones. Unfortunately, only three thumper shots were detected on pairs of geophones, and no thumper shots gave detectable first arrivals on all three geophones. Consequently, there was too little redundancy in the data to give reliable values for the relative geophone sensitivities, relative shot strengths or the exponent for the amplitude variation with separation. Only for the Apollo-16 ASE was there sufficient data to perform this analysis at all, and it indicated that there could be 30 to 40% variability in the geophone sensitivities and 15 to 20% variability in the thumper-shot strengths. An amplitude variation with separation equal to $x^{-3.6}$ was obtained from this analysis. It is not possible to give much credence to these values because the amplitudes used in this analysis were small and had large variability.

In conclusion, it has been demonstrated that the power-law-velocity model predicts: 1) the measured arrival times of the first arrivals as well as, if not better than, the layered-velocity model does and 2) the amplitude

variation with separation as well as that model does. The quality of the data does not allow a definitive choice to be made between the two models. However, the power-law model predicts a very low velocity at the lunar surface which, in turn, implies that seismic rays will be nearly normally incident to the surface. This would explain why there is little correlation between the vertical and horizontal components of the motions detected by the Passive Seismic Experiment seismometers. It also implies that the long duration of the seismic signals detected on the Moon is due to scattering by even shallow undulations of the surface (Gold and Soter, 1970 and Gargi, 1972). The power-law velocity model also predicts that the lunar regolith is composed of fine particles (soil) down to a depth of 5 to 6 meters. The power-law model indicates that the velocity below 6 meters is not "sampled" by the first arrivals detected over separations less than or equal to 32m.

Appendix A

Variation in amplitude with distance in a vertically inhomogeneous medium.—

An approximate analysis of the variation in amplitude of a compressional wave in a vertically inhomogeneous elastic medium can be made using ray theory. The analysis closely follows the developments given in Bullen (1963) and Officer (1958).

The analysis is approximate in that it does not take into account either the variation in waveform of the propagating wave (i.e., dispersion) or the conversion of p-wave energy into s-wave energy (these assumptions are also made in the above references).

We assume that, for a source on the surface, the energy, dE , contained in a "bundle of rays" with ray parameters between $p-dp/2$ and $p+dp/2$ is equal to the intensity (or energy per unit area), I , times the area subtended by the ray parameters (see Figure A.1a)

$$dE(p) = I(x', p) dA = S(p) dp \quad (A.1)$$

where

$I(x', p)$ = the wave intensity for a ray with ray parameter, p , at a horizontal distance, x' , away from the source point,

dA = area contained between the circular "cones" given by $p-dp/2 = \text{constant}$ and $p+dp/2 = \text{constant}$ ($dA = 2\pi x' dw$),

$S(p)$ = energy per unit change in the ray parameter,

p = the ray parameter = $\sin\theta(z)/v(z)$,

$\theta(z)$ = the angle between the ray and the vertical z axis and is measured counterclockwise from the z axis, and

$v(z)$ = the velocity variation with depth.

The intensity for any point along the ray can be expressed as

$$I(x', p) = \frac{S(p)}{2\pi x'} \frac{dp}{dw}. \quad (A.2)$$

At a fixed depth, z , and for a particular ray bundle centered about ray parameter p , (see Figure A.1b)

$$dw(x', p) = \cos \theta dx'; \quad \text{or} \quad \frac{dw}{dp} = \cos \theta \frac{dx'}{dp}. \quad (A.3)$$

When the ray reaches the surface ($z=0$), $\theta(0)=\pi$ ($\cos \theta(0)=-1$) and

$$x'(p, z=0) \equiv x(p). \quad (A.4)$$

The intensity at the surface receiver then becomes

$$I(x, p) = -\frac{S(p)}{2\pi x} \frac{dp}{dx}. \quad (A.5)$$

(Note, the intensity is positive since both $S(p)$ and x are positive but dp/dx is negative at the surface).

The general relationship for vertically inhomogeneous media

$$p = dt/dx \quad (A.6)$$

holds, where $t(x)$ is the travelttime; therefore we have

$$I(x, p) = \frac{S(p)}{2\pi x} \frac{d^2 t}{dx^2}. \quad (A.7)$$

It can be verified directly that $p=dt/dx$ for a velocity variation of the form

$$v(x) = v_0 (z/z_0)^n \quad (0 < n < 1) \quad (A.8)$$

by using: (1) the fact that

$$dt/dx = (dt/dp)/(dx/dp) \quad (A.9)$$

and (2) the parametric equations for the travelttime, $t(p)$, and the source/receiver separation, $x(p)$, (see, for example, Kaufman, 1953)

$$\begin{aligned} t(p) &= C_n p^{-(1-n)/n} \\ x(p) &= (1-n)C_n p^{-1/n} \end{aligned} \quad (\text{A.10})$$

where C_n is a constant equal to

$$C_n = \frac{2\sqrt{\pi}z_0}{nv_0^{1/n}} \frac{\Gamma(1/2n+1/2)}{\Gamma(1/2n)} \quad (\text{A.11})$$

The problem that remains in determining the intensity is to express $S(p)$ in terms of x . The rays from a source at the surface propagate, initially, vertically; therefore, for a vertical-force source, most of the energy will be directed along the z -axis with little or no energy propagating along the surface. The rays received at the surface near the source correspond to large values of the ray parameter p because

$$p = 1/v(z_T) \quad (\text{A.12})$$

where z_T is the turning depth of the ray; i.e., its maximum depth of penetration. Therefore, if we assume an asymptotic expansion for $S(p)$ of the form (for $p \gg 1$)

$$S(p) \sim p^{-m}(1 + 1/p + 1/p^2 + \dots); \quad m > 1 \quad (\text{A.13})$$

and use the fact that (from equation A.10)

$$p \sim x^{-n}$$

we have

$$S(p) \sim x^{mn}. \quad (\text{A.14})$$

This indicates that the source radiation pattern contributes an increase to the intensity as the separation increases. This is due to the fact that the rays detected at the larger separations come from

that part of the radiation pattern where the intensity is higher; namely, closer to the z-axis. In order to insure integrability of $S(p)$ for the large values of p ($1 \leq p < \infty$), the exponent m must be greater than 1.

Using the fact that

$$\frac{1}{x} \frac{d^2 t}{dx^2} \sim x^{-(n+2)} \quad (\text{A.15})$$

the intensity variation with separation x becomes

$$I(x) \sim x^{-[2+n(1-m)]} \quad (\text{A.16})$$

and the amplitude variation is

$$A(x) \sim I^{1/2} \sim x^{-[2+n(1-m)]/2}. \quad (\text{A.17})$$

For the self-compacting-powder model, $n=1/6$ and we have

$$A(x) = A(x_0) (x/x_0)^{-(13-m)/12}; \quad m > 1. \quad (\text{A.18})$$

Appendix B

The relative geophone sensitivities, shot strengths and the amplitude variation; least-squares analysis.

The optimum values, in a least-squares sense, of 1) the relative geophone sensitivities, 2) the relative shot strengths and 3) the exponent of the amplitude variation with distance can be determined if there is sufficient redundancy in the amplitude data and the functional form of the amplitude function is known. The direct-wave-amplitude variation has the functional form given by equation (6) both for a half space (i.e., constant velocity) and for a vertically inhomogeneous medium (i.e., $v(x,y,z) = v(z)$ only).

The summed, weighted and squared error, E^2 , between the log of the measured amplitude values and the values predicted by the functional form (as expressed in equation (8)) is (see equation (9)):

$$E^2(a_0, m, \bar{g}, \bar{s}) = \sum_{i=1}^I \sum_{j=1}^J w_{ij} (a_0 + mX_{ij} + g_i + s_j - a_{ij})^2 \quad (B.1)$$

where $a_0 = \log(G_I S_J)$, G_I is the reference-geophone sensitivity, S_J is the reference-shot strength, \bar{g} is the (vector of) relative geophone sensitivities, g_i is the relative sensitivity of the i -th geophone, \bar{s} is the (vector of) relative shot strengths, s_j is the relative strength of the j -th shot, X_{ij} is the log of the separation between the i -th geophone and the j -th shot and a_{ij} is the log of the amplitude measured at the i -th geophone for the j -th shot.

We define a parameter vector, \bar{p} , in the parameter space made up of the a_0 , g_i , s_j and m :

$$\bar{p} = \sum_{i=1}^I \hat{g}_i g_i + \sum_{j=1}^J \hat{s}_j s_j + \hat{m}m + \hat{a}_0 a_0 = \sum_{n=1}^{I+J+2} \hat{p}_n p_n = \bar{g} + \bar{s} + \bar{m} + \bar{a}_0 \quad (B.2)$$

where the symbols with carets above them (e.g., \hat{g}_i) are unit vectors in the parameter space. They are assumed to be orthogonal (or independent), that is:

$$\begin{aligned} \hat{p}_n \cdot \hat{p}_m &= \delta_{nm} \quad \text{or} \quad \hat{g}_i \cdot \hat{g}_k = \delta_{ik}, \quad \hat{s}_j \cdot \hat{s}_r = \delta_{jr}, \quad \hat{m} \cdot \hat{g}_i = \hat{m} \cdot \hat{s}_j = \\ \hat{m} \cdot \hat{a}_0 &= \hat{a}_0 \cdot \hat{g}_i = \hat{a}_0 \cdot \hat{s}_j = \hat{g}_i \cdot \hat{s}_j = 0. \end{aligned} \quad (B.3)$$

where, for example, δ_{ik} is the Kronecker delta which is defined as $\delta_{ik}=0$ if $i \neq k$, $\delta_{ik}=1$ for $i=k$. Therefore,

$$a_0 + mX_{ij} + g_i + s_j = \bar{p} \cdot (\hat{a}_0 + \hat{m}X_{ij} + \hat{g}_i + \hat{s}_j). \quad (B.4)$$

The summed, weighted and squared error, $E^2(\bar{p})$, will have a minimum in the parameter space where its gradient is zero; that is:

$$\frac{1}{2} \frac{\partial}{\partial \bar{p}} E^2 = \sum_i \sum_j w_{ij} (a_0 + mX_{ij} + g_i + s_j - a_{ij}) (\hat{a}_0 + \hat{m}X_{ij} + \hat{g}_i + \hat{s}_j) = 0 \quad (B.5)$$

or

$$\begin{aligned} \sum_i \sum_j w_{ij} a_{ij} (\hat{a}_0 + \hat{m}X_{ij} + \hat{g}_i + \hat{s}_j) \\ = \sum_i \sum_j w_{ij} [(\hat{a}_0 + \hat{m}X_{ij} + \hat{g}_i + \hat{s}_j) (\hat{a}_0 + \hat{m}X_{ij} + \hat{g}_i + \hat{s}_j)] \cdot \bar{p} \end{aligned} \quad (B.6)$$

where the term inside the brackets is a square, symmetric maxtrix obtained by the dyadic product of the two vectors (see equation (B.7), next page). The resulting set of equations can be written in matrix form as

$$\bar{a} = \bar{A} \cdot \bar{p} \quad (B.8)$$

(B.7)

$$\begin{aligned}
 \bar{A} = & \begin{bmatrix}
 \sum_{ij} w_{ij} & \sum_{ij} w_{ij} X_{ij} & \sum_j w_{1j} & \sum w_{2j} & \dots & \sum w_{i2} & \dots \\
 \sum_{ij} w_{ij} X_{ij} & \sum_{ij} w_{ij} X_{ij}^2 & \sum_j w_{1j} X_{1j} & \sum w_{2j} X_{2j} & \dots & \sum w_{i2} X_{i2} & \dots \\
 \sum_j w_{1j} & \sum_j w_{1j} X_{1j} & \sum_j w_{1j} & 0 & 0 \ 0 \ 0 & w_{12} & \dots \\
 \sum_j w_{2j} & \sum_j w_{2j} X_{2j} & 0 & \sum w_{2j} & 0 \ 0 \ 0 & w_{22} & \dots \\
 \vdots & \vdots & 0 & 0 & \begin{smallmatrix} 0 \ 0 \\ 0 \ 0 \\ 0 \ 0 \end{smallmatrix} & \vdots & \vdots \\
 \sum_i w_{i1} & \sum w_{i1} X_{i1} & w_{11} & w_{21} & \dots & \sum w_{i1} & 0 \ 0 \ 0 \\
 \sum_i w_{i2} & \sum w_{i2} X_{i2} & w_{12} & w_{22} & \dots & \sum w_{i2} & 0 \ 0 \ 0 \\
 \vdots & \vdots & \vdots & \vdots & \begin{smallmatrix} \vdots \\ \vdots \\ \vdots \end{smallmatrix} & 0 & \begin{smallmatrix} 0 \ 0 \\ 0 \ 0 \\ 0 \ 0 \end{smallmatrix}
 \end{bmatrix}
 \end{aligned}$$

where \bar{a} is the vector

$$\begin{aligned}\bar{a} &= \sum_n \hat{p}_n a_n \\ &= \sum_i \sum_j w_{ij} a_{ij} (\hat{a}_0 + \hat{m} X_{ij} + g_i + s_j)\end{aligned}\quad (B.9)$$

the square, symmetric matrix \bar{A} is defined in equation (B.7) and the vector \bar{p} is defined in equation (B.2).

The parameter values (\hat{a}_0, \hat{m}, g_i and s_j) are just the components of the vector \bar{p} and they are determined by inverting equation (B.8) to give

$$\bar{p} = \bar{A}^{-1} \cdot \bar{a}. \quad (B.10)$$

This is the solution to the problem of determining the optimum (in a least-squares sense) parameters and it can be seen from equation (B.10) that the accuracy of the solution depends upon the stability of the inverse of the matrix \bar{A} and the errors in the vector \bar{a} . These, in turn, depend upon the accuracy of the measurements of the separations, X_{ij} , and the amplitudes, a_{ij} , and the values of the weights, w_{ij} . The weights themselves are established by the accuracies of a_{ij} and X_{ij} . In the analysis of the amplitude data from the Apollo-16 ASE, it was assumed that the separations were measured with high accuracy; consequently, the weights were established only on the basis of the accuracy of the amplitude measurements.

From the form of matrix \bar{A} (equation (B.7)), it can be seen that it will have a stable inverse if there is high redundancy in the data; that is, the sums of the weights over the geophones (subscript i) and over the shot strengths (subscript j) as well as the double sums (over i and j) have large values. This will occur when the amplitude from each shot is measured accurately at each geophone; that is, all the $w_{ij}=1$. Unfortunately, this is not the case in the Apollo-14 or Apollo-16 ASE's.

References

- Bullen, K. E., An Introduction to the Theory of Seismology, Third Edition, Cambridge University Press, New York, N.Y., Chapter 8, (1963).
- Chang, G. K., P. Gunther and D. B. James, "A secondary ejecta explanation of a lunar seismogram," Jour. Geophys. Res., 75, pp. 7426-7438, 1970.
- Cooper, M. R., R. L. Kovach and J. S. Watkins, "Lunar near-surface structure", Reviews of Geophysics and Space Physics, 12, pp. 291-308, (1974).
- Dainty, A. M., M. N. Toksoz, K. R. Anderson, P. J. Pines, Y. Nakamura and G. Latham, "Seismic scattering and shallow structure of the Moon in Oceanus Procellarum", The Moon, 9, pp. 11-29, (1974).
- Gangi, A. F. "The lunar seismogram", The Moon, 4, pp. 40-48, (1972).
- Gassmann, F., "Elastic waves through a packing of spheres", Geophysics, 16, pp. 673-685 (1951). See also Geophysics, 18, p. 269 (errata), (1953).
- Gold, T. and S. Soter, "Apollo 12 seismic signal: indication of a deep layer of powder", Science, 169, pp. 1071-1075, (1970).
- Kaufman, H., "Velocity functions in seismic prospecting", Geophysics, 18, pp. 289-297, (1953).
- Kovach, R. L., J. S. Watkins, and T. Landers, "7. Active Seismic Experiment", Apollo 14 Preliminary Science Report, NASA SP-272, pp. 163-174, (1971).
- Kovach, R. L., J. S. Watkins, and P. Talwani, "10. Active seismic experiment", Apollo 16 Preliminary Science Report, NASA SP-315, pp. 10.1-10.14, (1972).
- Kovach, R. L. and J. S. Watkins, "The Velocity Structure of the Lunar Crust", The Moon, 7, pp. 63-75, (1973).
- Latham, G., M. Ewing, F. Press, G. Sutton, J. Dorman, Y. Nakamura, N. Toksoz, R. Wiggins, J. Derr and F. Duennebier, "Apollo 11 passive seismic experiment", Proceedings of the Apollo 11 Lunar Science Conference, Geochim. Cosmochim. Acta, Suppl. 1, 3, pp. 2309-2320, (1970a).

- Latham, G. V., M. Ewing, F. Press, G. Sutton, J. Dorman, Y. Nakamura, N. Toksoz, R. Wiggins, J. Derr and F. Duennebier, "Passive seismic experiment", Science, 167, pp. 455-457, (1970b).-
- Latham, G., M. Ewing, F. Press, G. Sutton, J. Dorman, Y. Nakamura, N. Toksoz, R. Wiggins and R. Kovach "3. Passive seismic experiment", Apollo 12 Preliminary Science Report, NASA SP-235, pp. 39-53, (1970c).
- Latham, G. V., M. Ewing, J. Dorman, F. Press, G. Sutton, R. Meissner, F. Duennebier, Y. Nakamura, R. Kovach and M. Yates, "Seismic data from man-made impacts on the moon", Science, 170, pp. 620-626, (1970d).
- Lauderdale, W. and W. Eichelman, Tech. Eds., "Active Seismic Experiment (NASA Experiment S-033)", Section 5, Apollo Scientific Experiments Data Handbook, NASA TMX-58131, 1974.
- Mukhamedzhanov, A. K., "The nature of the lunar seismic echo", translated from Piroda, 3, pp. 74-75 (1970) by E. R. Hope, Can. Tech. Sc., Moscow, Defence Scientific Information Service, DRB Canada, Translation T-542R, June, (1970).
- Officer, C. B., Introduction to the Theory of Sound Transmission, McGraw-Hill Book Co., Inc., New York, N. Y., pp. 49f, (1958).
- Sutton, G. H. and F. K. Duennebier, "Elastic properties of the lunar surface from Surveyor spacecraft data", J. Geophys. Res., 75, pp. 7439-7444, (1970).
- White, J. E., Seismic Waves, McGraw-Hill Book Co., Inc., New York, N. Y., p. 215, (1965).

TABLE I
Correspondence of binary data values (B.D.)
with the geophone voltage (V)
(Geophone 1, Apollo 16)

B.D.	V	B.D.	V	B.D.	V
0	-2.299	11	-.00363	22	+.02101
1	-1.279	12	-.00202	23	+.03783
2	- .7115	13	-.00112	24	+.06813
3	- .3958	14	-.00047	25	+.1227
4	- .2202	15	-.00000	26	+.2209
5	- .1225	16	+.00048	27	+.3978
6	- .06817	17	+.00111	28	+.7164
7	- .03793	18	+.00200	29	1.290
8	- .02110	19	+.00360	30	2.323
9	- .001174	20	+.00648	31	4.183
10	- .000653	21	+.01167		

Table II
Shot-to-Geophone Separations

Separation		No. of traces	Apollo-14 Shot Nos.*			Apollo-16 Shot Nos.*		
(ft)	(m)		GP-1	GP-2	GP-3	GP-1	GP-2	GP-3
0	0.00	6	21	11	1	19	11	1
15	4.57	5	20	12	2	-	10	2
30	9.14	7	19	13	3	18	9,12	3
45	13.71	6	18	-	4	17	8,13	4
60	18.29	6	17	7	-	16	7,14	5
75	22.86	4	-	-	-	15	6,15	6
90	27.43	6	-	17	7	14	5,16	7
105	32.00	6	-	4,18	-	13	4,17	8
120	36.58	7	13	3,19	-	12	3,18	9

*Thumper-shot numbers which had the proper separation from the three geophones.

Table III
Traveltimes (milliseconds)

Separation x(m)	Measured Traveltimes [§]					Calculated Traveltimes		
	1	2	3	4	5	A	B	C
4.57	55	53	56	52	-	51.7	44.0	40.1
9.14	91	91	-	87	99	92.1	87.9	80.2
13.71	123	123	124	-	128	129.1	131.9	120.3
18.29	151	149	152	-	155	164.2	175.8	160.4
22.86	-	-	-	-	177?	197.7	219.8	200.5
27.43	206?	230	196?	229	199?	230.1	*245.0	240.6
32.00	255?	274?	264?	274?	-	261.7	*260.3	280.7
1-n	.76	.80	.74	.84	.63	5/6	—	1
v _o (m/s)	590	430	630	340	1200	350	104	114

§ Times with question marks (?) indicate difficult time determinations

* Traveltimes of the first refracted wave (earliest arrival)

1. Measured from Apollo-14 and -16 stacked data (3-66 Hz)
2. Measured from Apollo-14 (only) stacked data (3-66 Hz)
3. Measured from Apollo-16 (only) stacked data (3-66 Hz)
4. Measured from Apollo-14, geophone-2 profile (3-66 Hz)
5. Measured from Apollo-16, geophone-1 profile (3-66 Hz)
- A. Self-compacting-powder model; $t=14.57 \times^{5/6}$ (msec.)
- B. Apollo-14 layered model (Kövach and Watkins, 1973)
- C. Apollo-16 layered model (Kövach and Watkins, 1973)

Table IV. Amplitude Data (arbitrary units)

A. Bandpassed: 3-66Hz

x (m.)	14-1 ⁺	14-2(1) [§]	14-3 ⁺	14-Σ [§]	16-1 ⁺	16-2(3) [§]	16-3 ⁺	16-Σ [§]	14,16-Σ [§]
4.57	4.62	3.91	4.68	4.19	-	5.82	5.34	4.69	3.95
9.14	3.17	2.08	?	3.36	1.43	.76	3.17	.82	1.16
13.71	1.13	*	?	1.13	.81	.32	.54	.31	.40
18.29	.52	*	*	.52	.56	.45	.42	.26	.30
22.86	*	*	*	*	?	.18?	.23?	?	?
27.43	*	.15	.1?	.17	.13	?	.18?	.10	.07
32.00	*	.10?	*	.10?	?	?	?	.19?	?
Slope	-1.55	-1.83	-2.15	-1.78	-1.77	-2.01	-2.01	-1.97	-2.04

B. Bandpassed: 20-40Hz

x (m.)	14-1 ⁺	14-2(1) [§]	14-3 ⁺	14-Σ [§]	16-1 ⁺	16-2(3) [§]	16-3 ⁺	16-Σ [§]
4.57	2.38	2.17	2.65	2.26	-	2.94	2.48	2.34
9.14	1.75	.93	1.49	1.75	.66	.39	1.70	.44
13.71	.56	*	.22	.56	.33	.20?	?	.17
18.29	.24	*	*	.24	.29	.22	.21	.13
22.86	*	*	*	*	?	?	.11	?
27.43	*	.13	.05	.09	.06	?	.10	.05
32.00	*	?	*	?	?	?	?	?
Slope	-1.63	-1.59	-2.34	-1.87	-2.07	-1.98	-2.00	-2.08

⁺14-1 means Geophone 1, Apollo-14 ASE, etc.; [§]14-Σ means stacked traces, Apollo-14 ASE
[§]14-2(1) means traces on Geophone 2, Apollo-14 ASE, sources between Geophones 1 and 2, etc.
 * misfired shot; -, no shot available; ?, low S/N ratio.

Table V - Data Weights and Separations; Apollo-16 ASE

Weights: w_{ij} Separations: $|x_i - x_j|$

Shot No. (j)	Geophone No. (i)		
	1	2	3
1	0	0	0
2	0	0	1
3	0	0	1
4	0	0	1
5	0	0	1
6	0	$\frac{1}{2}$	$\frac{1}{2}$
7	0	1	$\frac{1}{2}$
8	0	1	0
9	0	1	0
10	0	1	0
11	0	0	0
12	0	1	0
13	0	0	0
14	$\frac{1}{2}$	0	0
15	0	0	0
16	1	0	0
17	1	$\frac{1}{2}$	0
18	1	0	0
19	0	0	0

Geophone No. (i)		
1	2	3
91.44	45.72	0
86.87	41.14	4.57
82.30	36.58	9.14
77.72	32.00	13.71
73.15	27.43	18.29
68.58	22.86	22.86
64.05	18.29	27.43
59.44	13.71	32.00
54.86	9.14	36.58
50.29	4.57	41.14
45.72	0	45.72
36.58	9.14	54.86
32.00	13.71	59.44
27.43	18.29	64.05
22.86	22.86	68.58
18.29	27.43	73.15
13.71	32.00	77.72
9.14	36.58	82.30
0	45.72	91.44

List of Figure Captions

- Figure 1. Long-period, vertical component (LPZ) lunar seismograms, Apollo-11 Passive Seismic Experiment, 1969. (From Latham, et.al., 1970a).
- Figure 2. Seismic ray paths for a linearly increasing velocity variation with depth and topographic irregularities. (From Gold and Soter, 1970).
- Figure 3. Plan view of the geophone siting and thumper-shot locations for the Apollo-14 and Apollo-16 Active Seismic Experiments. (Geophones: o; shots: x; misfired shots: ■).
- Figure 4. Representative raw-data traces from the Apollo-16 ASE. (Thumper shot 10).
- Figure 5. "Deglitched" versions of the traces in Figure 4.
- Figure 6. Bandpass-filtered versions of the traces in Figure 4. (3db frequencies: 10.5 & 66.25Hz).
- Figure 7. Amplitude spectrum of the first two seconds of the signal from geophone 2, thumper shot 10, Apollo-16 ASE. (Separation: 4.57m).
- Figure 8. Stacked, filtered and amplified traces for shot-to-geophone separations of 0, 4.57 and 9.14m. (Apollo-14 and Apollo-16 signals combined; Bandpass: 10.5 to 66Hz).
- Figure 9. Stacked, filtered and amplified ASE profile (Apollo-14 and Apollo-16 signals combined; Bandpass: 20 to 50Hz).
- Figure 10. Single-geophone profile, filtered and amplified. (Geophone 1, Apollo-16 ASE; Bandpass: 20 to 50Hz).
- Figure 11. Log-log plot of the traveltimes versus separations for the stacked and filtered traces. (Apollo-14 and Apollo-16 ASE signals combined; Bandpass: 3 to 66Hz; measured slope: $m=0.76$ and reference velocity: $v_0=590\text{m/sec}$).

List of Captions (Con't.)

Figure 12. log-log plot of the amplitudes versus separations (Single geophone amplitudes; Geophone 3, Apollo-16 ASE; Bandpass: 3 to 66Hz; measured slope: -2.01).

Figure A-1. a) Ray paths for a power-law velocity variation: $v(z)=v_0(z/z_0)^n$.
b) Detail of the wavefront, dw, in a ray bundle.

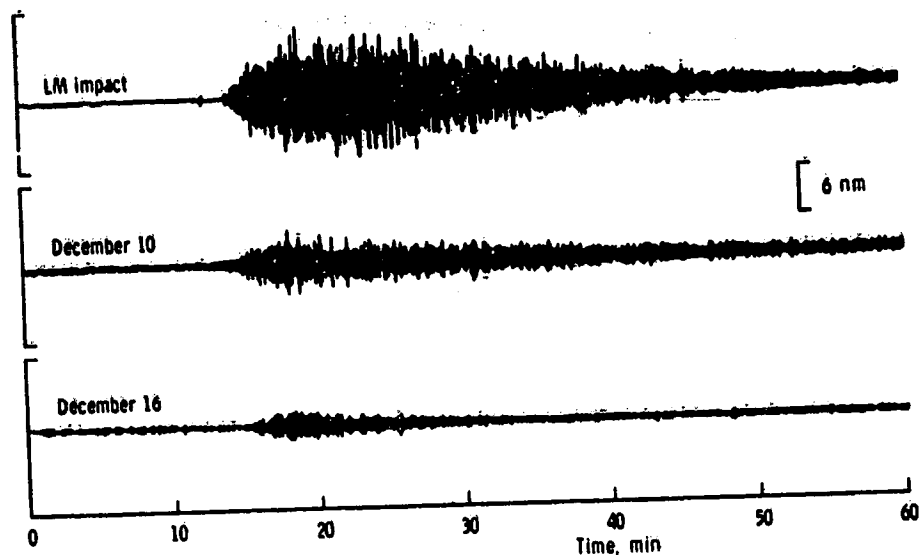


Figure 1. Long-period, vertical component (LPZ) lunar seismograms, Apollo-11 Passive Seismic Experiment, 1969. (From Latham, et.al., 1970a).

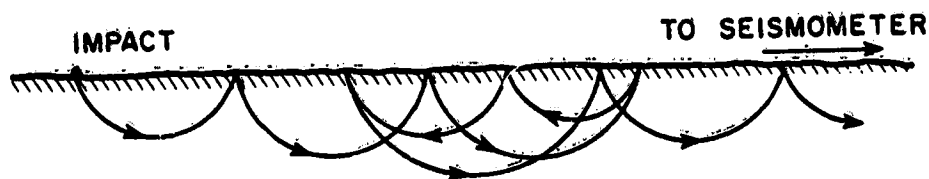
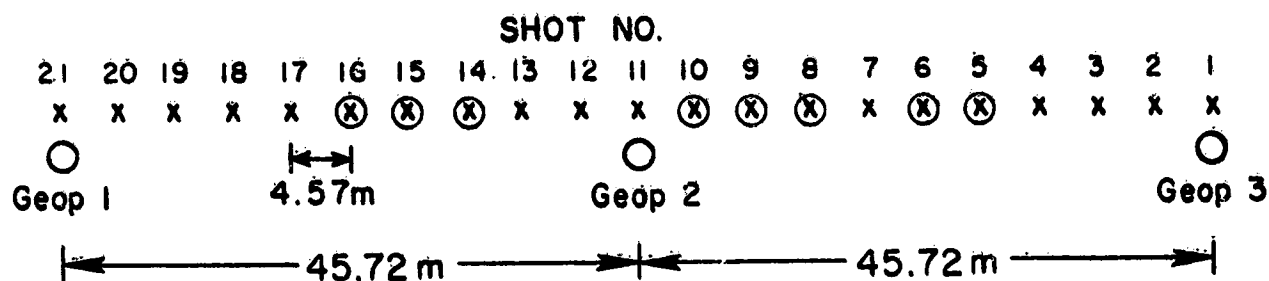
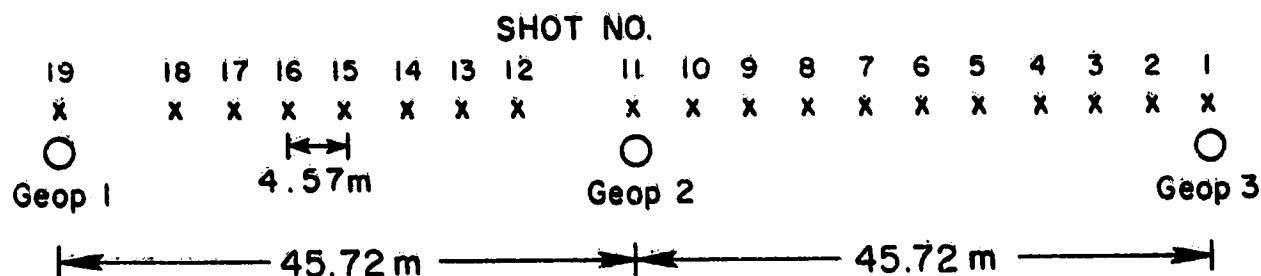


Figure 2. Seismic ray paths for a linearly increasing velocity variation with depth and topographic irregularities. (From Gold and Soter, 1970).



a) APOLLO-14 ACTIVE SEISMIC EXPERIMENT. (21 shots)
 Shots 5, 6, 8, 9, 10, 14, 15 and 16 misfired.



b) APOLLO-16 ACTIVE SEISMIC EXPERIMENT. (19 shots)

Figure 3. Plan view of the geophone siting and thumper-shot locations for the Apollo-14 and Apollo-16 Active Seismic Experiments. (Geophones: o; shots: x; misfires: ■).

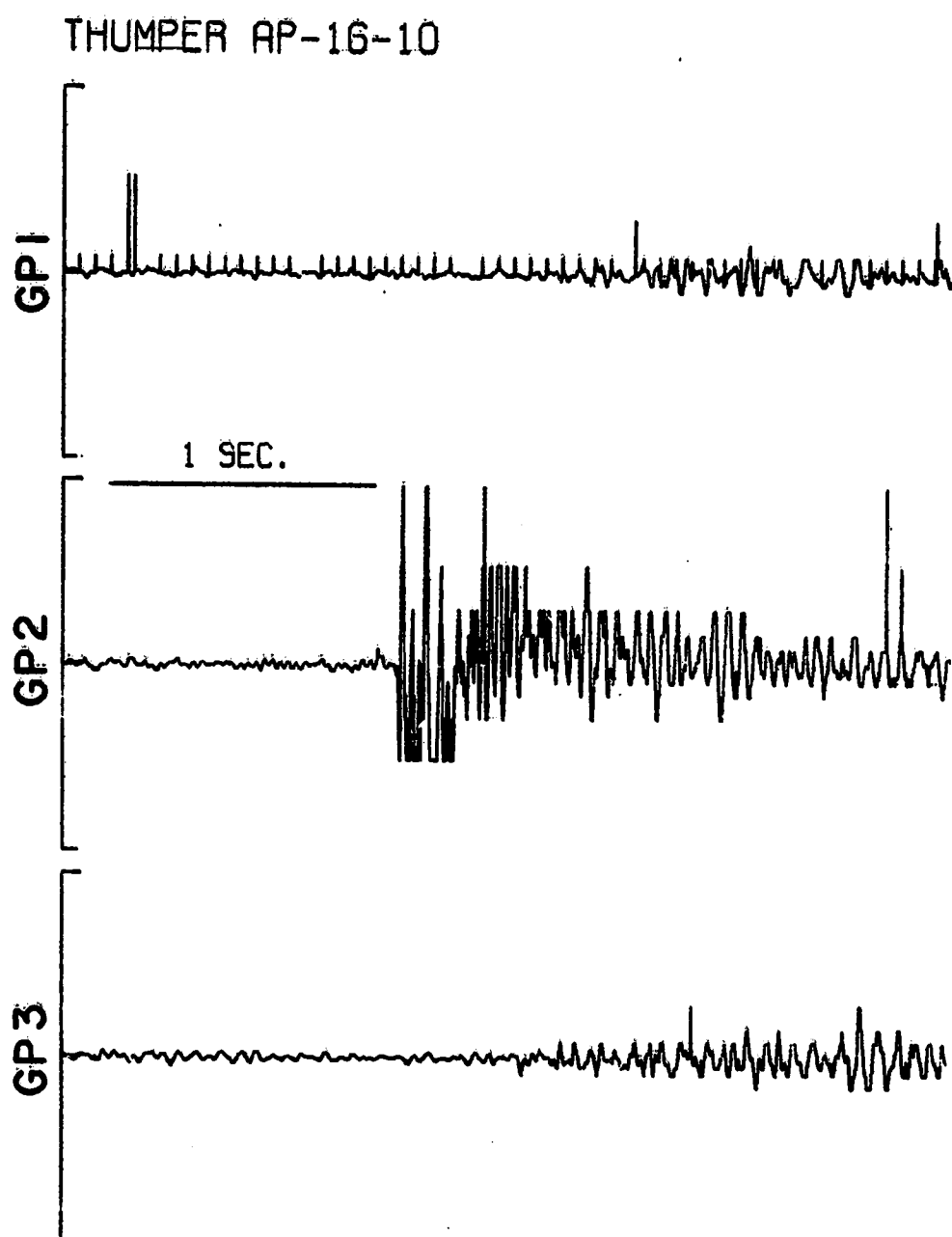


Figure 4. Representative raw-data traces from the Apollo-16 ASE. (Thumper Shot 10).

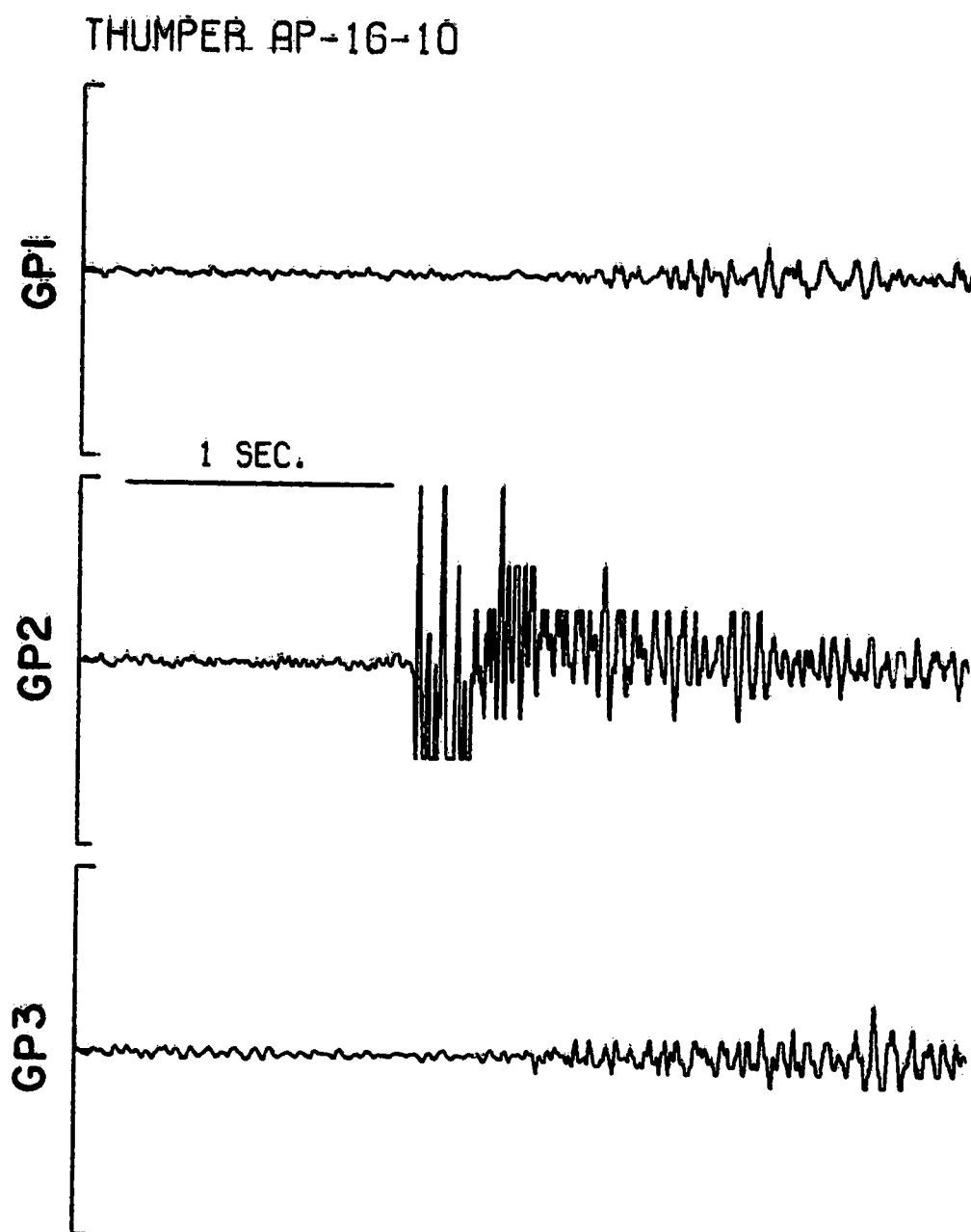


Figure 5. "Deglitched" versions of the traces in Figure 4.

THUMPER AP-16-10 FILTERED

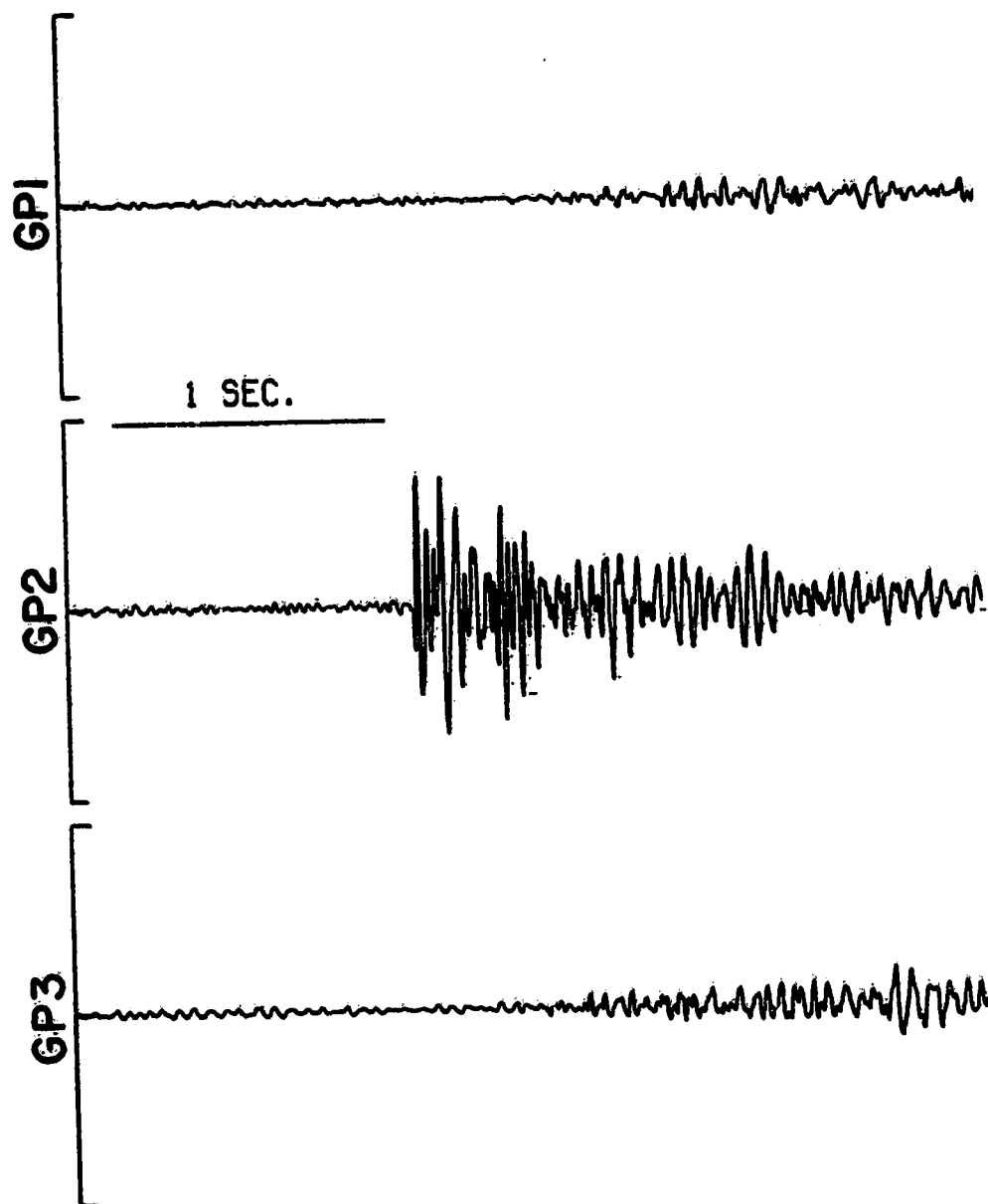


Figure 6. Bandpass-filtered versions of the traces in Figure 4.
(3 db frequencies: 10.5 & 66.25 Hz).

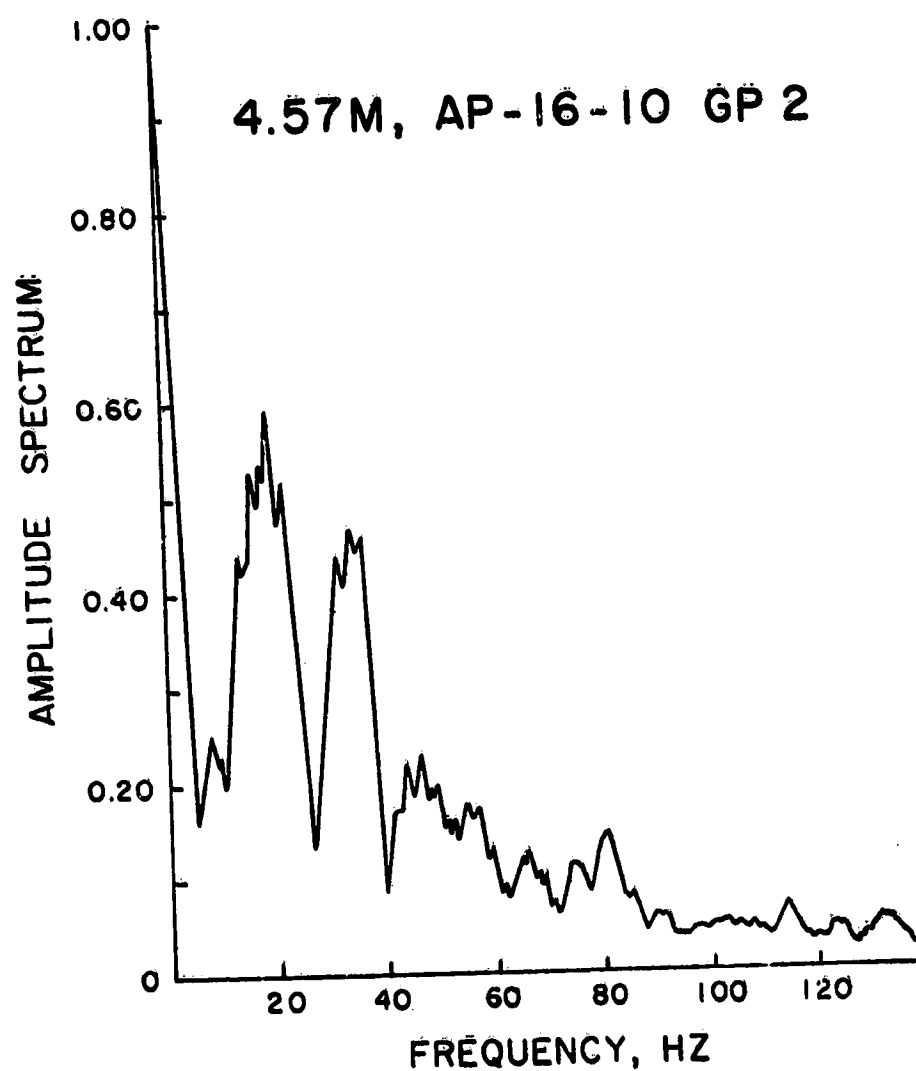


Figure 7. Amplitude spectrum of the first two seconds of the signal from geophone 2, thumper shot 10, Apollo-16 ASE. (Separation: 4.57 m).

STACKED, FILTERED AND AMPLIFIED

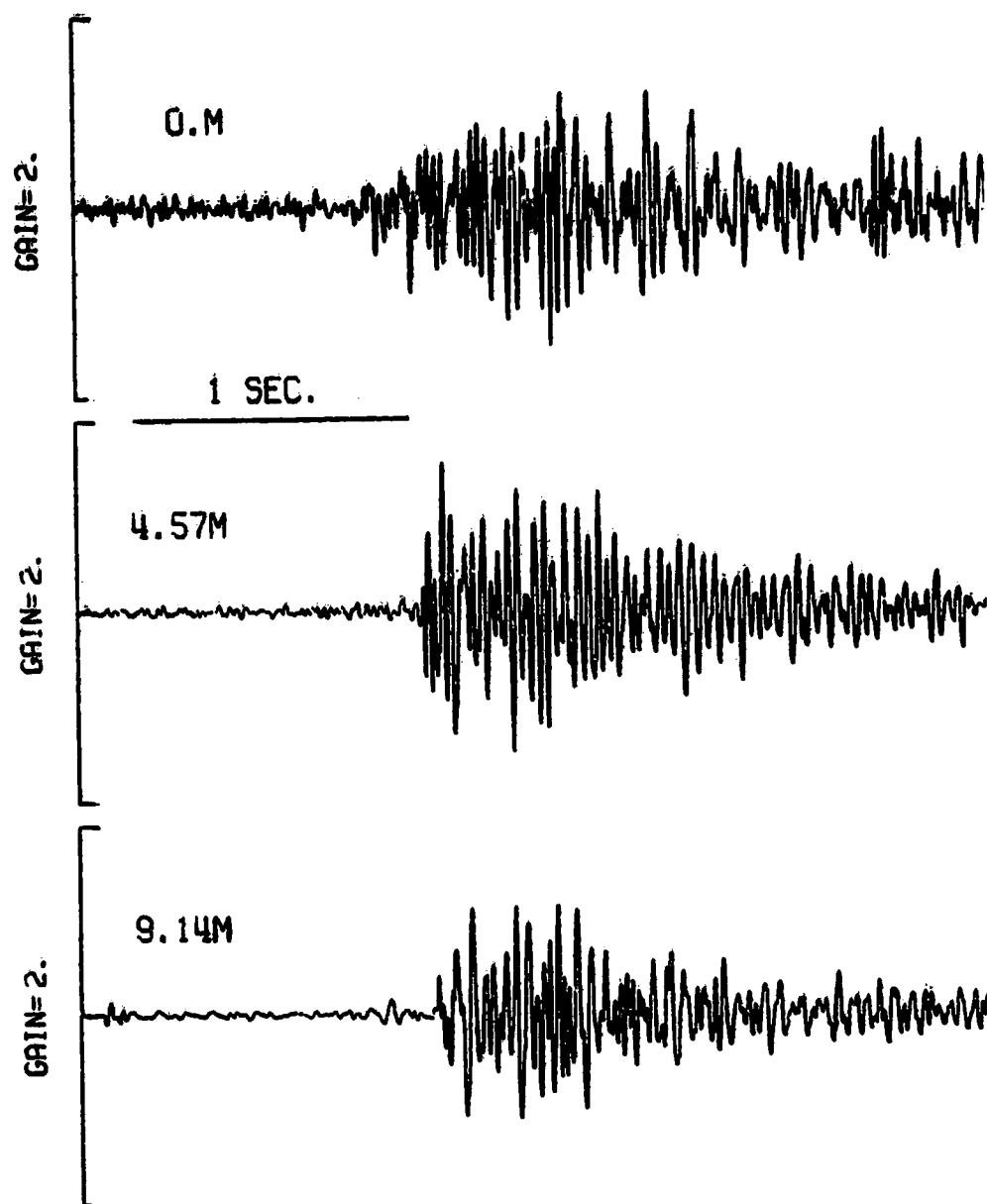


Figure 8. Stacked, filtered and amplified traces for shot-to-geophone separations of 0, 4.57 and 9.14 m. (Apollo-14 and Apollo-16 signals combined; Bandpass: 10.5 to 66 Hz).

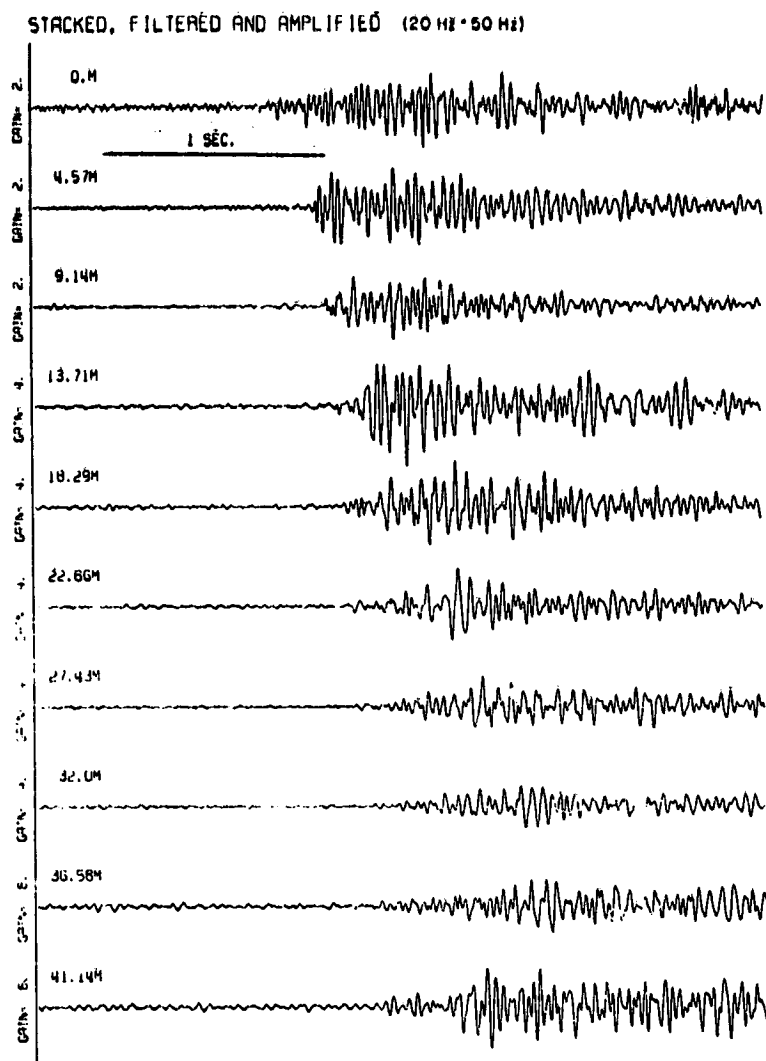


Figure 9. Stacked, filtered and amplified ASE profile (Apollo-14 and Apollo-16 signals combined; Bandpass: 20 to 50 Hz).

ORIGINAL PAGE IS
OF POOR QUALITY

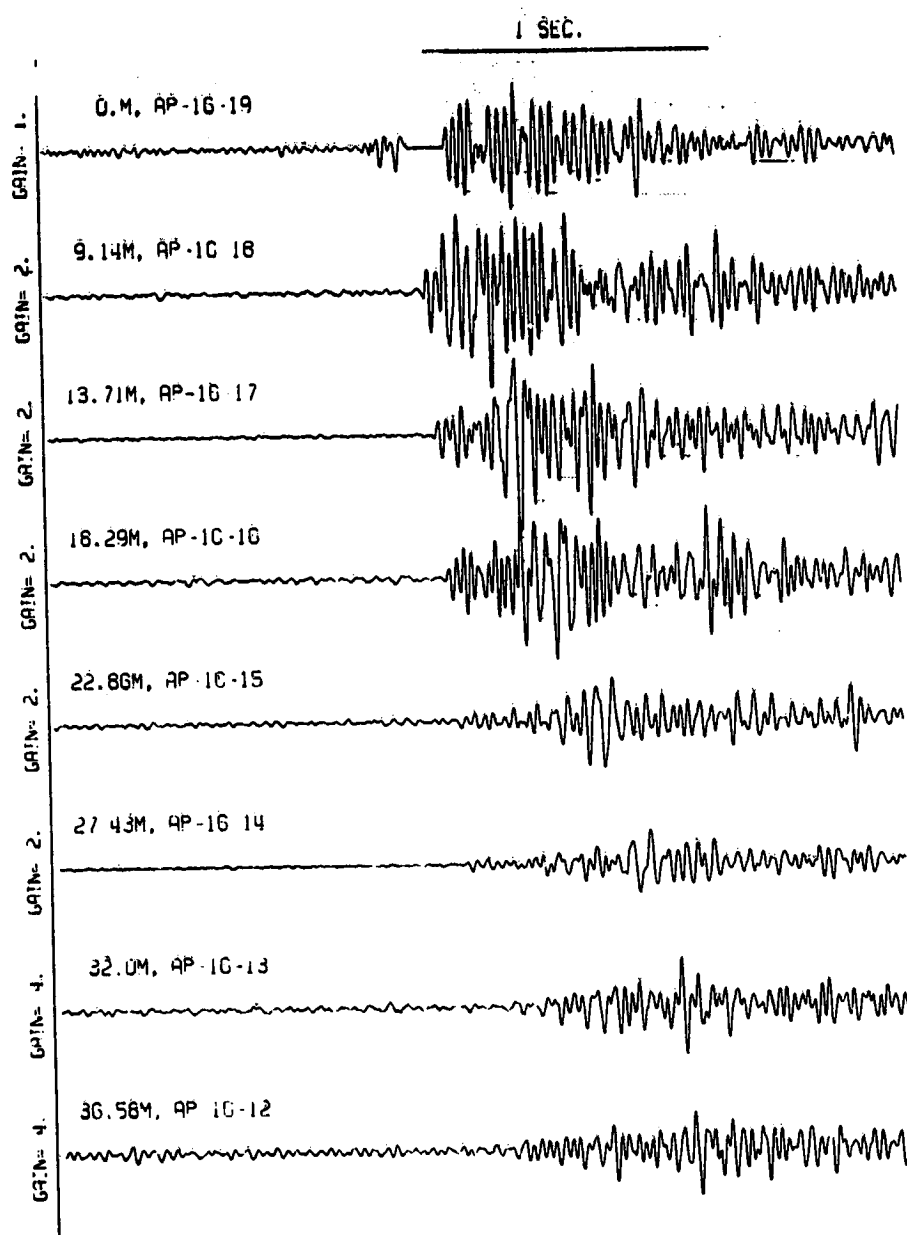


Figure 10. Single-geophone profile, filtered and amplified.
(Geophone 1, Apollo-16 ASE; Bandpass: 20 to 50 Hz).

ORIGINAL PAGE IS
OF POOR QUALITY

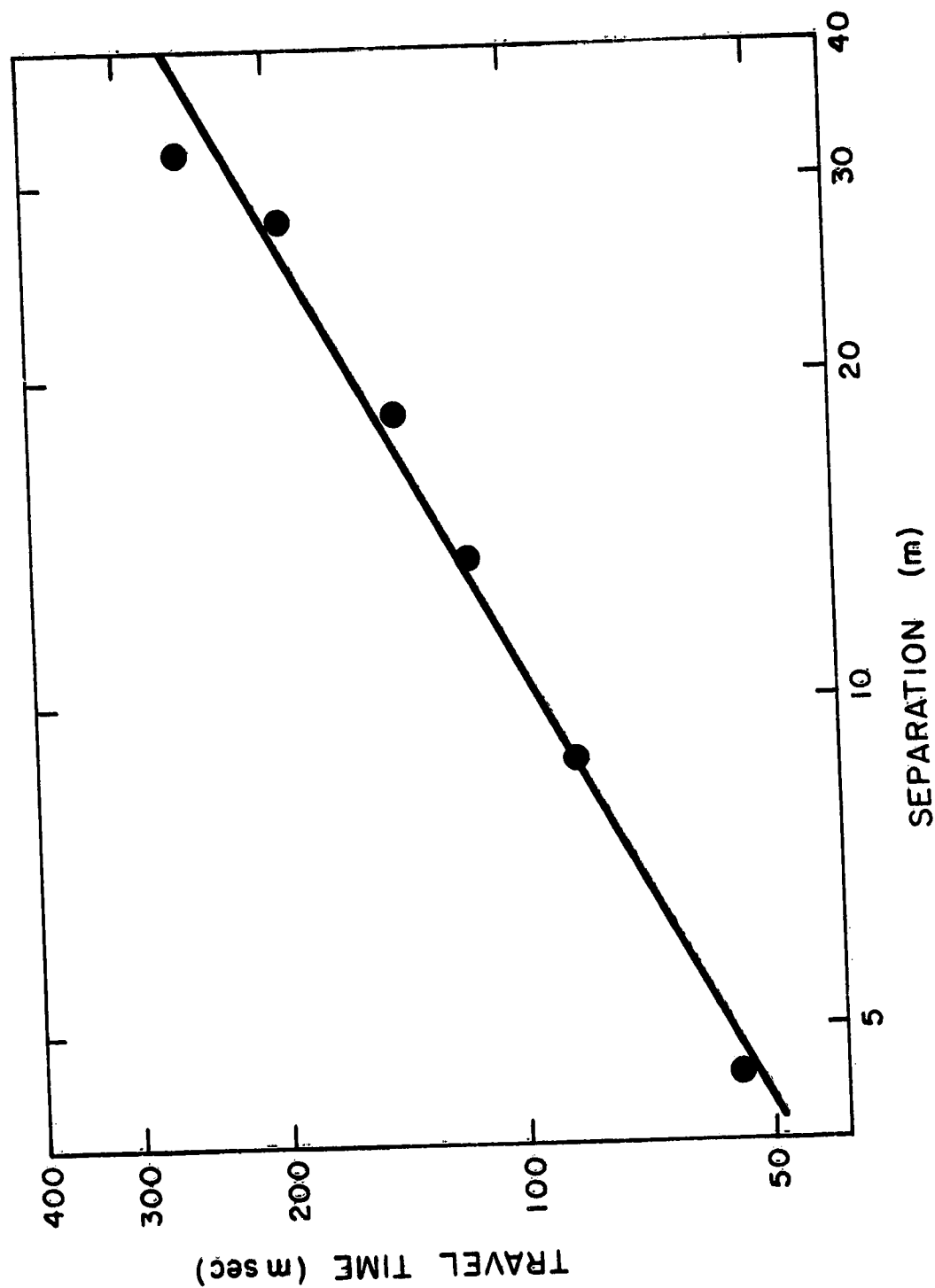


Figure 11. Log-log plot of the traveltimes versus separations for the stacked and filtered braced. (Apollo-14 and Apollo-16 ASE signals combined; Bandpass: 3 to 66 Hz; measured slope: $m=0.76$ and reference velocity: $v_0=590$ m/sec).

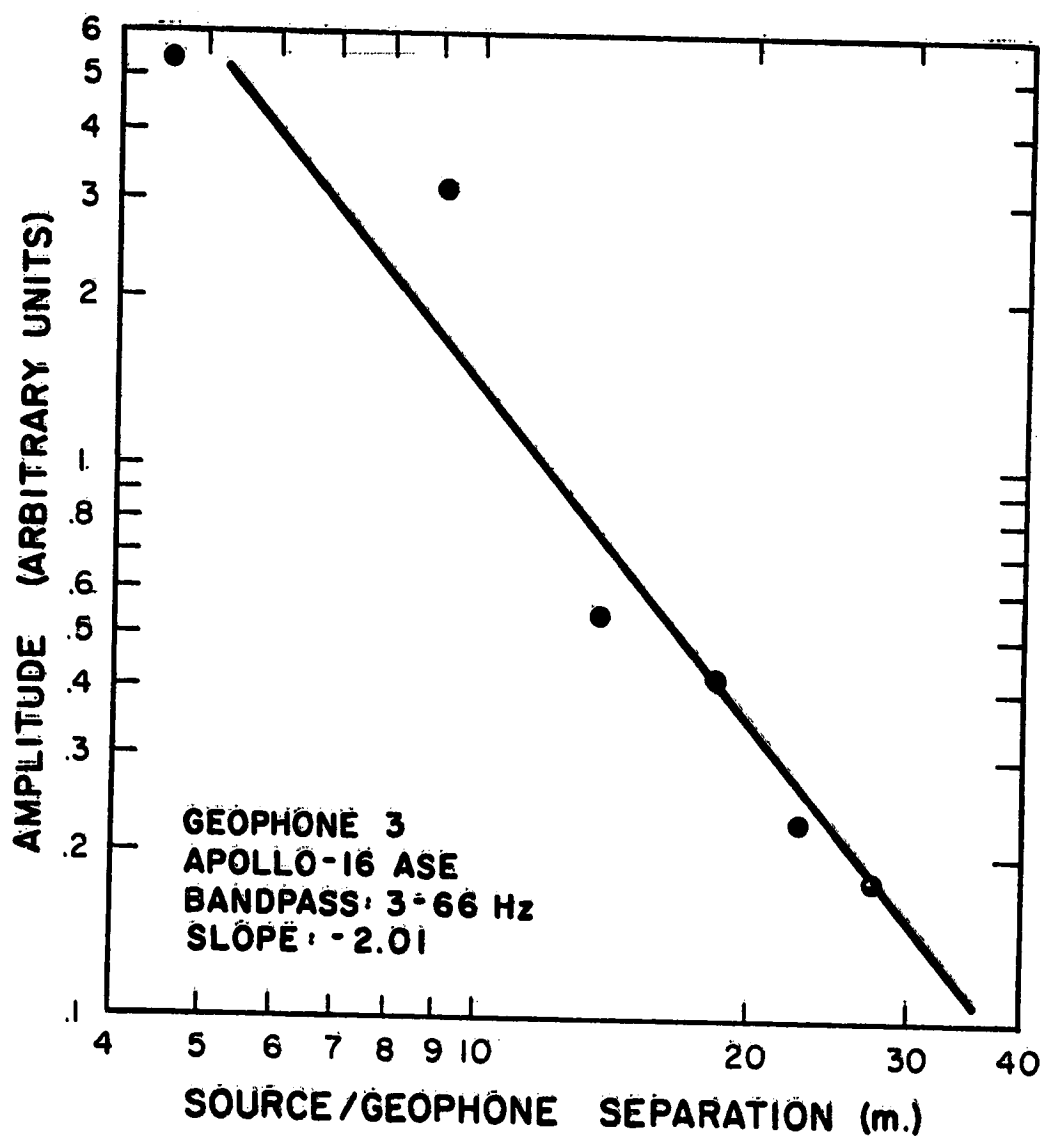


Figure 12. Log-log plot of the amplitudes versus separations (single geophone amplitudes; Geophone 3, Apollo-16 ASE; Bandpass: 3 to 66 Hz; measured slope: -2.01).

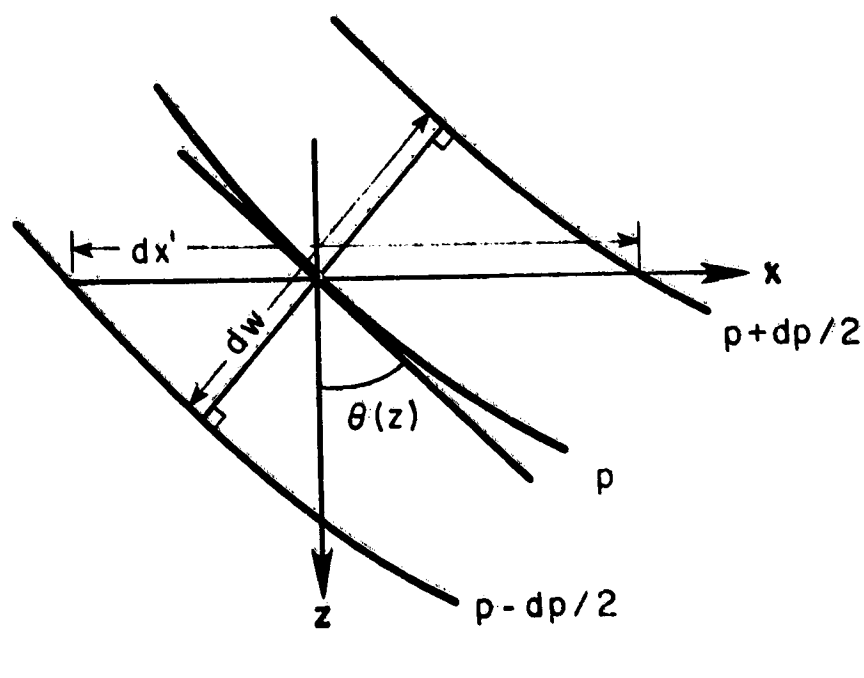
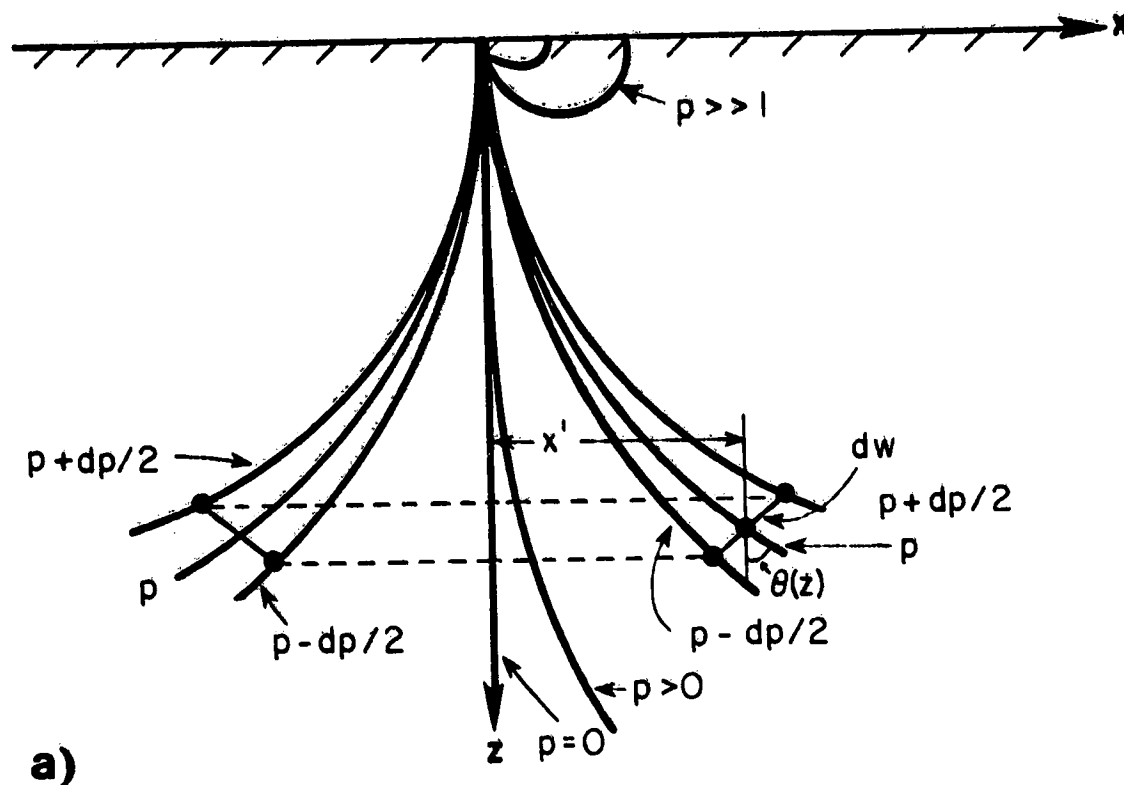


Figure A-1. a). Ray paths for a power-law velocity variation:
 $v(z) = v_0(z/z_0)^n$.
 b). Detail of the wavefront, dw , in a ray bundle.